THE GEOLOGICAL SOCIETY OF AMERICA®

Timing of deep-water slope evolution constrained by large-*n* detrital and volcanic ash zircon geochronology, Cretaceous Magallanes Basin, Chile

Benjamin G. Daniels[1,†], Neal C. Auchter[2], Stephen M. Hubbard[1], Brian W. Romans[2], William A. Matthews[1], and Lisa Stright[3]

[1]*Department of Geoscience, University of Calgary, 2500 University Drive NW, Calgary, Alberta T2N1N4, Canada*
[2]*Department of Geosciences, Virginia Tech, 926 West Campus Drive, Blacksburg, Virginia 24061, USA*
[3]*Department of Geosciences, Colorado State University, 1482 Campus Delivery, Fort Collins, Colorado 80523-1482, USA*

ABSTRACT

Deciphering depositional age from deposits that accumulate in deep-water slope settings can enhance understanding of shelf-margin evolutionary timing, as well as controlling mechanisms in ancient systems worldwide. Basin analysis has long employed biostratigraphy and/or tephrochronology to temporally constrain ancient environments. However, due to poor preservation of index fossils and volcanic ash beds in many deep-water systems, deducing the timing of slope evolution has proven challenging. Here, we present >6600 new U-Pb zircon ages with stratigraphic information from an ~100-km-long by ~2.5-km-thick outcrop belt to elucidate evolutionary timing for a Campanian–Maastrichtian slope succession in the Magallanes Basin, Chile. Results show that the succession consists of four stratigraphic intervals, which characterize four evolutionary phases of the slope system. Overall, the succession records 9.9 ± 1.4 m.y. (80.5 ± 0.3 Ma to 70.6 ± 1.5 Ma) of graded clinoform development punctuated by out-of-grade periods distinguished by enhanced coarse-grained sediment bypass downslope. Synthesis of our results with geochronologic, structural, and stratigraphic data from the basin suggests that slope evolution was largely controlled by an overall decline in basin subsidence from 82 to 74 Ma. In addition to providing insight into slope evolution, our results show that the reliability of zircon-derived depositional duration estimates for ancient sedimentary systems is controlled by: (1) the proportion of syndepositionally formed zircon in a stratigraphic interval; (2) the magnitude of the uncertainty on interval-bounding depositional ages relative to the length of time evaluated; and (3) the geologic time (i.e., period/era) over which the system was active.

INTRODUCTION

Linked delta to deep-water slope systems characterized by long-term (≥1 m.y.) progradation are commonly represented by thick (hundreds to thousands of meters) stratigraphic successions (e.g., Carvajal and Steel, 2009; Dixon et al., 2012). Occurrences of thick sandstone-prone turbiditic packages within siltstone-prone slope successions have been interpreted as evidence for enhanced coarse-grained sediment delivery to the deep ocean over ≥1 m.y. periods (cf. Mutti and Normark, 1987; Stevenson et al., 2015; Romans et al., 2016). These periods, which can be initiated by autogenic processes such as shelf-edge delta migration (e.g., Mellere et al., 2002; Porębski and Steel, 2003), or by allogenic mechanisms such as eustatic sea-level change or tectonism (e.g., Piper and Normark, 1989; Nelson et al., 2011), can characterize distinct evolutionary phases of slope systems. Other examples of slope evolutionary phases include periods of mass wasting and readjustment (cf. Coleman and Prior, 1988; Masson et al., 2006) and propagation of slope clinothems (cf. Rich, 1951; Hedberg, 1970; Ross et al., 1994).

Though many workers have provided key insights into slope evolution through the analysis of ancient (e.g., Uchupi and Emery, 1967; Hadler-Jacobsen et al., 2005; Houseknecht et al., 2009) and modern systems (e.g., Wynn et al., 2000; Mulder et al., 2014), information on the timing and duration of slope evolutionary phases is limited. Elucidating the timing of slope systems provides insight into the mechanisms that initiated and propagated phases of their evolution (cf. Carvajal et al., 2009; Callec et al., 2010). Understanding the timing of episodic terrigenous sediment delivery to the deep sea at ≥1 m.y. time scales enables the use of turbidite archives to study shifts in terrestrial climate (e.g., Clift and Gaedicke, 2002; Romans et al., 2016; Covault et al., 2010), sedimentary system responses to tectonic perturbations (e.g., Martinsen et al., 1999), and land-sea linkages in general (e.g., Romans and Graham, 2013). Moreover, many ancient slope deposits serve as prolific hydrocarbon reservoirs (e.g., Mayall et al., 2006; Weimer and Pettingill, 2007), and a greater comprehension of slope evolution timing can potentially improve reservoir prediction on continental margins worldwide.

The ability to temporally constrain deep-time slope evolution has been difficult, in part, because of the lack of high-resolution depositional age-dating techniques suitable to slope system succession and intra-slope-system succession (e.g., slope clinothem) scales. Biostratigraphy can offer robust chronologic constraints in some slope systems (e.g., Pinous et al., 2001; Johannessen and Steel, 2005); however, its ability to resolve distinct slope evolution phases is limited, because in situ microfossils may not be present or equally abundant in all parts of a slope system (cf. Piper, 1975; McHugh et al., 1996). U-Pb zircon geochronology has also been used to add temporal insight into slope evolution (e.g., Fildani et al., 2007; Bernhardt et al., 2012). Though detrital U-Pb zircon ages from sandstone beds have been used to constrain shelf-edge development (e.g., Schwartz et al., 2016), the way in which the timing of shelf-edge evolution relates to corresponding slope evolutionary phases is a topic of ongoing research (Carvajal et al., 2009; Prather et al., 2017). U-Pb zircon ages from volcanic ash layers can provide

†bgdaniel@ucalgary.ca

GSA Bulletin; ; https://doi.org/10.1130/B31757.1; 10 figures; 1 table; Data Repository item 2017304.

precise depositional age information; however, ash layers in high-sediment-flux, deep-water slope systems are commonly poorly preserved (e.g., Plink-Björklund et al., 2001; Bain and Hubbard, 2016).

To better understand the temporal characteristics of slope evolution, we determined maximum depositional ages of sandstone-prone units within slope strata of the Tres Pasos Formation and deltaic deposits of the Dorotea Formation, Magallanes Basin, Chile. This study employed large-*n* (>500 grains per sample) U-Pb detrital zircon geochronology calibrated with ages from two volcanic ash deposits, and these data were integrated with results of previous analyses in the basin (Romans et al., 2010; Bernhardt et al., 2012; Schwartz et al., 2016). The strata investigated is a 2500-m-thick Campanian–Maastrichtian siliciclastic succession composed of shelf through deep-water slope deposits associated with a high-relief (>1000 m) slope system (cf. Hubbard et al., 2010; Romans et al., 2011). The study objectives were to: (1) use field mapping and chronologic data to construct a stratigraphic framework for the ancient slope system and identify slope evolutionary phases; (2) document the timing and duration of component evolutionary phases; (3) use the results to investigate controlling mechanisms on slope evolution; and (4) evaluate the feasibility of U-Pb zircon geochronology approaches in the temporal characterization of ancient zircon-rich sedimentary systems.

GEOLOGIC SETTING

The Magallanes Basin, also known as the Austral Basin, is an elongate, north-south–oriented retroarc foreland basin that spans the southern regions of Chilean and Argentine Patagonia (Fig. 1). The basin is associated with Early Cretaceous–Neogene orogenesis of the southern Patagonian Andes (Dalziel et al., 1974; Natland et al., 1974; Wilson, 1991; Fildani and Hessler, 2005; Fosdick et al., 2011). The development of the basin was linked to a dynamic Mesozoic tectonic history in southernmost South America, including: (1) a Jurassic–Early Cretaceous extensional phase associated with the initial breakup of Gondwana, which resulted in the formation of the Rocas Verdes backarc basin (Pankhurst et al., 2000; Fildani and Hessler, 2005); and (2) a Late Cretaceous–Neogene compressional phase, which led to the development of a pronounced foredeep eastward of the Andean front (Fildani et al., 2003; Fildani and Hessler, 2005; Fosdick et al., 2011; Malkowski et al., 2017).

The extensional phase of tectonic evolution in southern Patagonia resulted in crustal attenuation in the Rocas Verdes Basin axis, which was most pronounced in the southern half of the basin (de Wit and Stern, 1981; Stern et al., 1992; Mukasa and Dalziel, 1996; Stern and de Wit, 2003; Romans et al., 2010; Malkowski et al., 2016). Extension in the Rocas Verdes Basin ceased due to the development of the compressional Andean fold-and-thrust belt, driven by increased spreading rates in the South Atlantic Ocean and associated subduction along the Pacific margin of South America (Bruhn and Dalziel, 1977; Rabinowitz and La Brecque, 1979; Dott et al., 1982; Dalziel, 1986; Ramos, 1988; Wilson, 1991).

The rapid uplift of the Andes and an inherited attenuated lithosphere led to enhanced subsidence and associated accommodation in the foredeep zone of the basin (Romans et al., 2010; Calderón et al., 2012; Fosdick et al., 2014). As a result, sediment derived from denudation during orogenesis was deposited in deep-water environments with water depths >1000 m (Natland et al., 1974; Hubbard et al., 2010). The deep-water depositional history of the Magallanes Basin in Chile is recorded by the Punta Barrosa, Cerro Toro, and Tres Pasos Formations (Fig. 1); the strata record the progressive infilling of the basin by orogen-parallel depositional systems that drained to the south during the Cretaceous (Winn and Dott, 1979; Shultz et al., 2005; Hubbard et al., 2008; Romans et al., 2011).

The Tres Pasos Formation is a Campanian–Maastrichtian siliciclastic unit primarily composed of deep-water slope deposits (Fig. 1; Smith, 1977; Shultz et al., 2005; Armitage et al., 2009; Romans et al., 2009; Hubbard et al., 2010). Slope clinoform surfaces in the Tres Pasos Formation can, in some places, be correlated updip into deposits of the genetically linked Dorotea Formation, a Campanian–Danian siliciclastic unit of shallow-marine to continental origin (Fig. 1; Hubbard et al., 2010; Bauer, 2012; Gutiérrez et al., 2017). Together, the two formations form the focus of this study and record deep-water basin infilling via evolution of a shelf-margin system (Macellari et al., 1989; Romans et al., 2009; Covault et al., 2009; Hubbard et al., 2010; Schwartz et al., 2016).

The Tres Pasos and Dorotea Formations are exposed along a discontinuous, north-south–oriented outcrop belt, which extends for ~140 km from the north shore of Lago Argentino in Argentina to Puerto Natales in Chile. This study focused on an ~100-km-long segment of the transect located between Cerro Divisadero in the north and Arroyo Hotel in the south (Fig. 1). Both formations are exposed along an eastward-dipping monocline on the eastern margin of the Andean fold-and-thrust belt; as such, a depositional-dip–oriented perspective is afforded by the lengthy outcrop belt (Hubbard et al., 2010).

METHODS

Field Mapping Techniques

Field mapping included measuring stratigraphic sections and photomosaic analysis, and these were complemented by surveying key stratigraphic surfaces using a differential global positioning system (GPS). Both measured section and GPS data were recorded at decimeter scale. Examination of satellite imagery enhanced stratigraphic correlations over long distances (i.e., tens of kilometers). Mapping was augmented with paleocurrent data, which were derived from measurements of sole marks, imbricated clasts, and ripples (total measurement $n = 5747$). Relatively flat, extensive, and chronostratigraphically equivalent units of the Dorotea Formation at the top of the succession were used as stratigraphic datums. These surfaces provided a reference for estimation of minimum relief on the ancient basin margin.

Zircon Geochronology

Detrital zircon samples ($N = 13$) were collected from sandstone units spanning the Tres Pasos and Dorotea Formations. Fine-grained sandstone was preferentially targeted for sampling (cf. Sláma and Košler, 2012). Zircon-bearing volcanic ash samples (15-ECB-01 and 15-CS-02) were collected at locations on Cerro Cazador and Cerro Solitario (Fig. 1; Table 1); both ash layers were located within successions of interbedded sandstone and siltstone turbidites on either side of the lithostratigraphic base of the Tres Pasos Formation.

Detrital zircon grains were isolated using standard mineral separation techniques (Fedo et al., 2003; Gehrels et al., 2008). U-Pb ratios and ages ($n = 6660$) were determined at the University of Calgary via conventional laser ablation–inductively coupled plasma–mass spectrometry (LA-ICP-MS) analytical methods (Gehrels et al., 2008; Matthews and Guest, 2017). For each sample, zircon populations were first analyzed using a high-throughput ($n > 500$), short-ablation-period ($t = 5$ s per grain) method; the youngest grains ($n \approx 30$ per sample) were then repolished and ablated for a longer time period ($t = 20$ s per grain) to reduce the uncertainty of each grain age. Where possible, grains in each youngest age population that could accommodate multiple 33 µm beam spots were ablated several times to better characterize grain age and to assess the potential for Pb loss (Gehrels, 2012; Spencer et al., 2016). Details of the

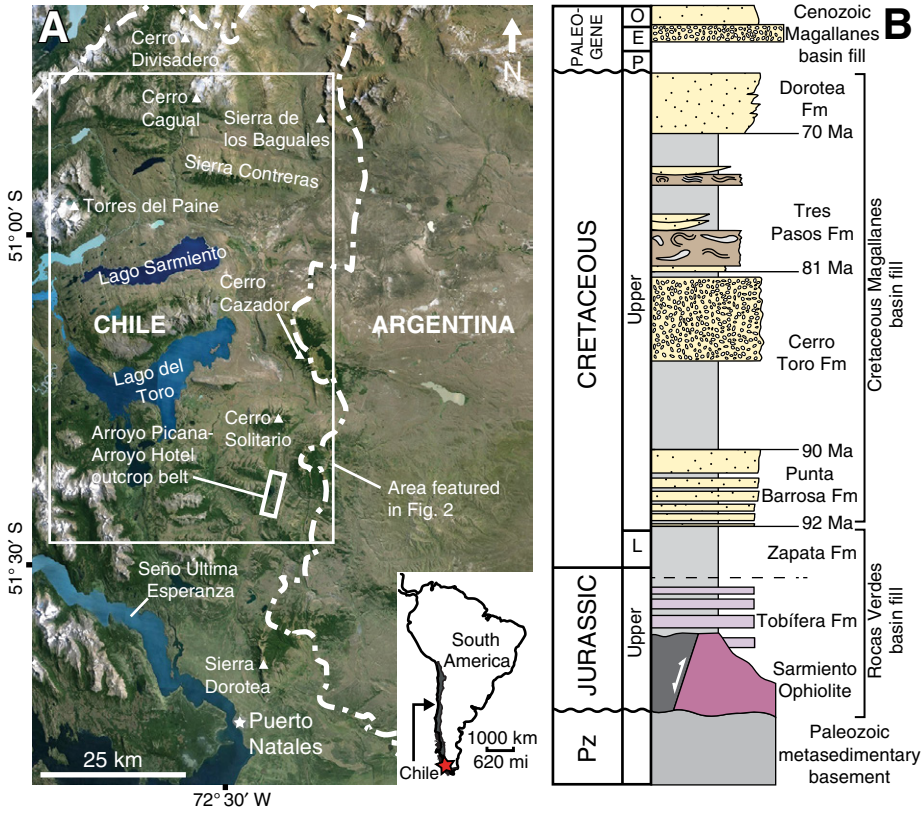

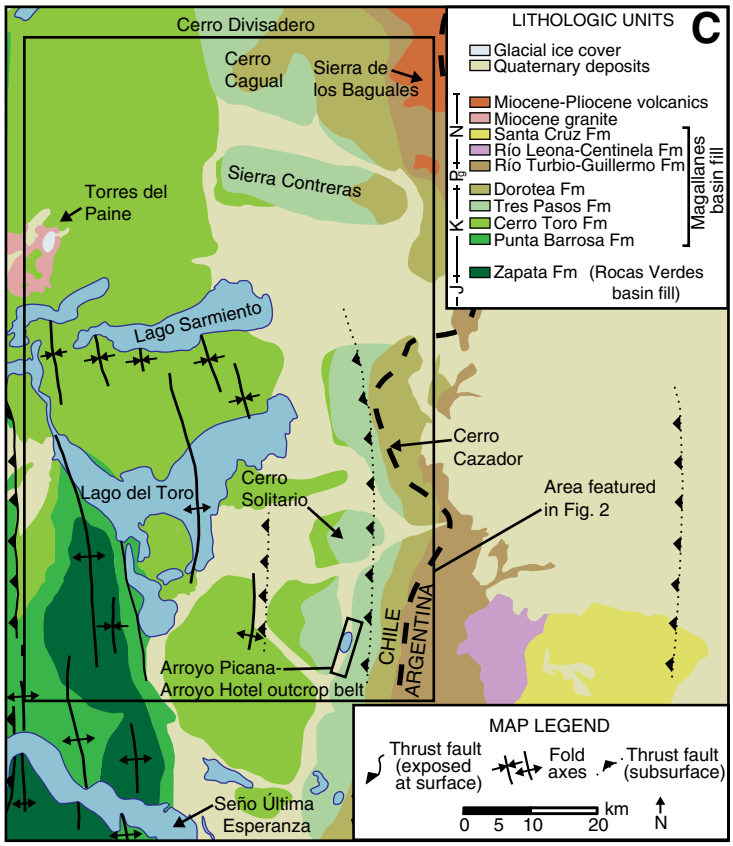

Figure 1. Overview of the Magallanes Basin in Última Esperanza Province, Chile. (A) Satellite image with key geographic features referenced in this study indicated (image data: Google, Landsat, Copernicus, 2016, http://www.google.com/earth/index.html, center of image coordinates: 51°11′21.72″S, 72°28′26.82″W). (B) Stratigraphic column of the Rocas Verdes and Magallanes Basin fill in Última Esperanza Province. Abbreviations in the figure refer to the following: Pz—Paleozoic; L—Lower; P—Paleocene; E—Eocene; O—Oligocene. Characteristic lithology (yellow—sandstone/conglomerate; brown—mass-transport deposit; gray—siltstone; light/dark purple—volcanogenic units) and architecture (channel form, tabular) for each formation are displayed (modified from Wilson, 1991; Fildani and Hessler, 2005; Fosdick et al., 2011; Schwartz et al., 2016). (C) Geologic map of the study area (modified from Fosdick et al., 2011). Abbreviations in the map legend refer to the following: J—Jurassic; K—Cretaceous; P_g—Paleogene; N—Neogene.

mineral separation and LA-ICP-MS procedures are presented in Appendix 1.[1]

Volcanic ash–derived zircon grains were isolated using standard mineral separation techniques (Fedo et al., 2003; Gehrels et al., 2008). U-Pb ratios and ages were determined via standard thermal ionization mass spectrometry (TIMS) analytical methods at the University of Arizona (cf. Saleeby et al., 1987; Davis et al., 2003; Otamendi et al., 2009). Details of the TIMS procedures are presented in Appendix 1 (see footnote 1).

Depositional Age Calculation

Sandstone maximum depositional ages (MDAs) employed dates presented in Appendix 2 (see footnote 1), and they were determined via weighted mean age calculations executed using Isoplot 4.15 in Microsoft Excel (Ludwig, 2012). In all cases, dates derived from $^{206}Pb/^{238}U$ ratios with a probability of concordance >1% were used (cf. Ludwig, 1998). MDAs were derived

[1]GSA Data Repository item 2017304, a summary of the geochronology methods (Appendix 1), the raw U-Pb dates (Appendix 2), and the results of the Monte Carlo simulations used to determine depositional duration values (Appendix 3), is available at http://www.geosociety.org/datarepository/2017 or by request to editing@geosociety.org.

TABLE 1. SANDSTONE AND VOLCANIC ASH SAMPLE INFORMATION

Sample name	Latitude (°S)	Longitude (°W)	Elevation (m)	Stratigraphic interval (SI)	MDA (YC2σ; Ma)	MDA (YGMA; Ma)	Description
15-CC-01	51°16′15.58″	72°19′57.86″	264	SI-4	70.6 ± 1.5	70.8 ± 1.8	Fine-grained sandstone
15-PIC-01	51°23′11.89″	72°22′04.33″	285	SI-4	73.9 ± 1.4	73.0 ± 10	Fine-grained sandstone
15-PIC-02	51°22′23.90″	72°23′28.38″	243	SI-4	74.3 ± 1.5	77.0 ± 14	Fine-grained sandstone
15-CAZ-01	51°08′12.20″	72°23′57.84″	1015	SI-4	75.2 ± 1.7	74.7 ± 1.5	Fine-grained sandstone
15-PIC-03	51°21′55.36″	72°23′56.67″	223	SI-4	80.2 ± 1.8	81.1 ± 4.8	Fine-grained sandstone
15-CAZ-02	51°08′09.33″	72°24′56.98″	890	SI-2	75.7 ± 1.7	73.7 ± 1.8	Fine-grained sandstone
15-PIC-04	51°21′41.96″	72°25′27.30″	190	SI-2	77.4 ± 1.1	77.0 ± 1.7	Fine-grained sandstone
15-RZ-DZ2	50°47′26.56″	72°41′39.33″	570	SI-2	78.0 ± 1.3	N.D.†	Fine-grained sandstone
15-CAZ-03	51°09′27.87″	72°25′37.18″	525	SI-2	81.2 ± 1.5	80.8 ± 1.8	Fine-grained sandstone
15-RZ-DZ3	50°46′11.55″	72°41′51.19″	948	SI-2	86.2 ± 2.1	N.D.†	Fine-grained sandstone
15-RZ-DZ1	50°47′32.97″	72°42′11.71″	354	SI-1	78.5 ± 1.3	78.7 ± 1.4	Fine-grained sandstone
15-CS-02	51°16′27.22″	72°27′28.68″	775	SI-1	80.5 ± 0.3	N.D.†	Volcanic ash deposit
15-CS-01	51°15′12.42″	72°26′41.02″	555	SI-1	80.6 ± 1.4	81.5 ± 1.6	Fine-grained sandstone
15-CAZ-04	51°10′16.85″	72°26′28.64″	175	SI-1	80.7 ± 1.5	N.D.†	Fine-grained sandstone
15-ECB-01	51°09′14.39″	72°28′22.88″	371	C.T.*	82.8 ± 0.3	N.D.†	Volcanic ash deposit

Notes: MDA—maximum depositional age; YC2σ—youngest cluster of dates (n ≥ 3) in a sample that overlapped at 2σ uncertainty; YGMA—youngest grain with multiple analyses. Samples that did not have grains that could be ablated multiple times with a 33 µm beam have an N.D. (not determined) designation in the YGMA column. Zircons from volcanic ash deposits were not ablated multiple times via thermal ionization mass spectrometry (TIMS); as such, YGMA MDAs for these samples also have an N.D. designation.

*C.T.—Cerro Toro Formation.

from the weighted mean age of the youngest cluster of dates ($n \geq 3$) in a sample that overlapped at 2σ uncertainty (YC2σ; Dickinson and Gehrels, 2009). These MDAs incorporated excess variance associated with heterogeneity in reference materials used in the zircon analysis (ε and ε′), as well as systematic uncertainty related to U-Pb ratios (e.g., $^{206}Pb/^{238}U$), U-Pb decay constants, and the ratio used to correct for ^{204}Pb in each analysis (Horstwood et al., 2016). This MDA calculation method employs individual grain dates from the youngest population, as well as weighted mean ages derived from multiple measurements on individual grains in the youngest population where possible. The weighted mean age from the youngest grain with multiple analyses (YGMA) provided another estimate of MDA for each sample (cf. Spencer et al., 2016); we also used these ages to verify results computed via the YC2σ MDA calculation technique.

Volcanic ash layer depositional ages also employed dates presented in Appendix 2 (see footnote 1), and they were determined from weighted mean age calculations executed with Isoplot 4.15 in Microsoft Excel (Ludwig, 2012). Dates derived from $^{206}Pb/^{238}U$ ratios were also used in each depositional age calculation. The ages represent the weighted mean of 12–13 TIMS dates from the youngest grains in each sample population.

Since the amount of syndepositionally formed zircon from hinterland sources present in sediment-routing systems can vary, zircon-derived MDAs can only provide an estimate of true depositional age (TDA; e.g., Dickinson and Gehrels, 2009; Rubio-Cisneros and Lawton, 2011). The absence of syndepositionally formed zircon in a system may result in computation of YC2σ and YGMA MDAs that are much older than the TDA (cf. Dickinson and Gehrels, 2009). Calculation of MDAs that are younger than TDA may also occur if a significant amount of Pb loss has occurred in the youngest zircons. In this study, YC2σ MDAs were preferred because they represent conservative estimates of TDA (Dickinson and Gehrels, 2009).

Depositional Rates

Our estimates of depositional age enabled the calculation of aggradation and progradation rates for various intervals within the stratigraphic succession. The time variable in each rate calculation was determined via Equation 1:

$$t = t_1 - t_2, \quad (1)$$

where t corresponds to the depositional duration of a given interval in the succession (m.y.), and each t_x variable corresponds to the bounding MDA of that interval (Ma, $t_1 > t_2$). Each t_x has an associated 2σ uncertainty value, which allows for the calculation of a range of t values. Each range of t values was calculated via a Monte Carlo simulation, where, using the 2σ uncertainty values associated with each bounding MDA, a synthetic population of 1000 ages was generated (Appendix 3, see footnote 1). Values of t were then determined for each pair of ages ($n_{pairs} = 1000$) in the population via Equation 1; the mean value ± 2σ of the results is reported to quantify the range of t values in each instance.

Shelf-margin aggradation and progradation rates were determined for stratigraphic intervals where shelf-edge positions could be defined; shelf-edge positions were defined where shallow marine topset deposits transitioned basinward to slope deposits. To characterize shelf margin growth, we used progradation and aggradation rates derived from Equations 2 and 3, respectively:

$$PR = D/t, \quad (2)$$

and

$$AR = T/t, \quad (3)$$

where PR = progradation rate (km/m.y.), AR = aggradation rate (m/m.y.), D = distance (km), and T = thickness (m). D is the distance from the initial shelf-edge position associated with one phase to the first shelf-edge position associated with the subsequent phase, and T is the thickness of sediment that accumulated between each shelf-edge position (Petter et al., 2013).

Shelf-margin growth rates utilized distances and thicknesses computed from the mapped stratigraphic framework. The calculations did not incorporate parameters related to the subsidence and accommodation histories of each phase, or the effects of burial and sediment compaction on each stratigraphic interval, because these data remain poorly constrained.

RESULTS

The results of this study include stratigraphic correlations and MDAs summarized in a regional-scale, dip-oriented cross section of the basin fill (Fig. 2), as well as a series of probability density plots, which display the distribution of zircon dates from each sample location

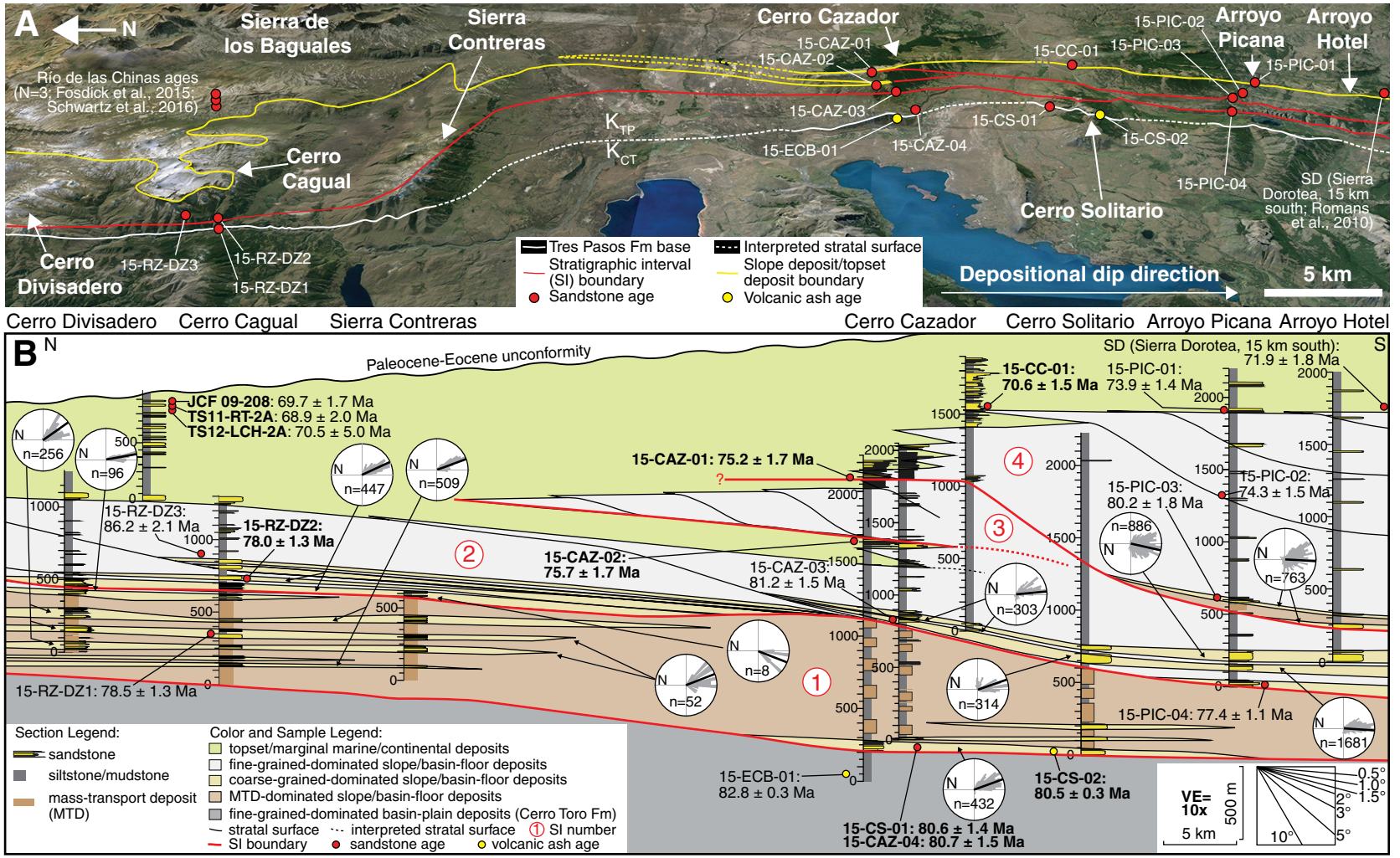

Figure 2. Campanian–Maastrichtian stratigraphic framework of the shelf-slope system studied. Paleoflow was from left to right (north to south). Correlation is based on field mapping augmented with U-Pb ages collected for this study, as well as other sources (Romans et al., 2010; Fosdick et al., 2015; Schwartz et al., 2016). (A) Perspective satellite image of the studied outcrop belt, looking down tectonic dip to the east (image data: Google, Centre National d'Études Spatiales, Astrium, Landsat, Copernicus, 2016, http://www.google.com/earth/index.html, center of image coordinates: 51°4'2.14"S, 72°37'30.47"W). Geochronology sample locations are indicated in red (detrital zircon) and yellow (ash). (B) Regional cross section of the shelf-margin system. Fine-grained–dominated deposits are largely composed of siltstone; coarse-grained–dominated deposits are largely composed of sandstone. All sample ages were computed from the weighted mean of the youngest cluster of dates that overlap within 2σ uncertainty (YC2σ) with the exception of the three ages from the Río de las Chinas area, which were determined from the weighted mean of the youngest cluster of dates that overlap within 1σ uncertainty (YC1σ; from Fosdick et al., 2015; Schwartz et al., 2016). Bold ages were used to calculate rates of shelf-margin growth in this study. Rose diagrams were derived from paleocurrent measurements of Armitage et al. (2009), Romans et al. (2009), Fletcher (2013), Macauley and Hubbard (2013), Hubbard et al. (2014), Daniels (2015), Pemberton et al. (2016), and Reimchen et al. (2016), with added information from this study. Measured section information collected for this study was augmented with data from Armitage et al. (2009), Romans et al. (2009), Hubbard et al. (2010), Bauer (2012), and Schwartz and Graham (2015). VE—vertical exaggeration.

(Fig. 3). The use of large numbers of grains to calculate each MDA (up to n = 12) commonly enabled depositional age determination with 2σ uncertainty <2 m.y. (Fig. 2; Table 1). These measurements, when combined with field mapping, resulted in development of a robust stratigraphic framework for the ancient shelf-slope succession (Fig. 2B; Hubbard et al., 2010; Bauer, 2012). The framework consists of four distinct stratigraphic intervals (Fig. 2B), which we examined for insight into paleoslope evolution.

Stratigraphic Interval 1 (SI-1)

Within the Tres Pasos Formation, the basal stratigraphic interval (SI-1) is characterized by thick (>100 m) accumulations of chaotically bedded siltstone-prone material intercalated with sandstone-prone turbiditic units (up to 90 m thick) that are tabular to lenticular in geometry (Fig. 2B; Armitage et al., 2009; Romans et al., 2009; Auchter et al., 2016). The sandstone-prone units commonly lap out onto the chaotically bedded deposits. SI-1 deposits associated with shallow-marine processes are not exposed in the study area, but they have been identified 70 km to the north (Arbe and Hechem, 1984; Macellari et al., 1989). The maximum thickness of SI-1 is ~800 m; overall, the thickness of SI-1 decreases from north to south (Fig. 2B). Three sandstone samples (15-CS-01, 15-CAZ-04, 15-RZ-DZ1) and one volcanic ash sample (15-CS-02) were analyzed from this interval; one ash from just below the base of this interval was also analyzed (15-ECB-01; Table 1; Fig. 2). Detrital zircon dates from this interval range from 3177.1 ± 74.4 Ma to 74.3 ± 7.1 Ma (Fig. 3; Appendix 2, see footnote 1). Depositional ages (i.e., sandstone-derived MDAs and volcanic ash ages computed via the YC2σ method) from within and just below this interval range from 82.8 ± 0.3 Ma to 78.5 ± 1.3 Ma (Fig. 2; Table 1).

Interpretation

The chaotically bedded deposits in SI-1 are related to periods of mass wasting on the paleoslope (cf. Coleman and Prior, 1988). The onlap relationship between the turbiditic units and the chaotically bedded strata suggests that the deposition of coarse-grained material was significantly influenced by seafloor topography created during mass wasting (Armitage et al., 2009; Auchter et al., 2016). Stacked successions of mass transport and turbiditic deposits are commonly associated with slopes that have undergone extended cycles of oversteepening and readjustment (Ross et al., 1994; Hadler-Jacobsen et al., 2005; Prather et al., 2017).

The ash from the uppermost part of the Cerro Toro Formation (15-ECB-01; 82.8 ± 0.3 Ma; Figs. 2B and 4) yielded an age that is toward the young end of the previously determined depositional age range for the unit in the study area (Bernhardt et al., 2012). The lowermost depositional ages from SI-1 (15-CAZ-04, 15-CS-01, and 15-CS-02) span 80.7 ± 1.5 Ma to 80.5 ± 0.3 Ma; these ages are within the bounds of the previously determined Tres Pasos Formation age range (Figs. 2B, 4, and 5; Natland et al., 1974; Macellari, 1988). Due to the highly precise and absolute time constraints offered by volcanic ash–derived zircon ages, we consider the 15-CS-02 volcanic ash age (80.5 ± 0.3 Ma), which is from within the basal sandstone-prone package of the Tres Pasos Formation, to most closely approximate the onset of coarse-grained sediment delivery. Notably, the ash and detrital zircon ages at the base of the Tres Pasos Formation overlap at 2σ uncertainty (Figs. 2B, 4, and 5), confirming that detrital zircons were routed to the basin shortly after crystallization. The youngest deposits sampled from within this interval (15-RZ-DZ1) yielded an age of 78.5 ± 1.3 Ma (Fig. 4); however, they are not from the top of the stratigraphic package. Sample 15-RZ-DZ2 is from just above the upper SI-1 contact and was thus used for rate calculations (Fig. 2B). Interval duration simulations, considering the 15-CS-02 age at the base of the interval (80.5 ± 0.3 Ma) and the 15-RZ-DZ2 age at the top (78.0 ± 1.3 Ma), indicate that SI-1 deposition spanned 2.5 ± 1.4 m.y. (Figs. 4 and 6).

Stratigraphic Interval 2 (SI-2)

The second stratigraphic interval of the shelf-slope succession is capped by shallow-marine deposits, which pinch out southward at Cerro Cazador (Fig. 2B). The lowest part of the section is characterized by dominantly siltstone-prone

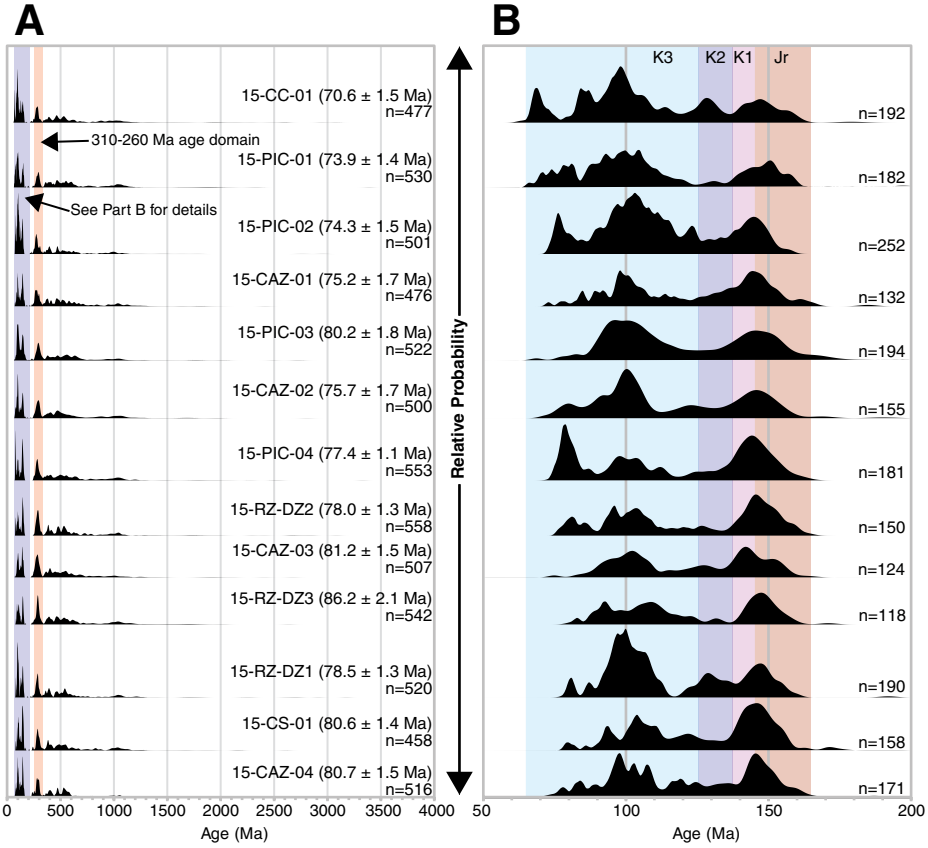

Figure 3. Normalized probability density plots of detrital zircon dates from each sample in this study, including (A) all accepted dates, and (B) all $^{206}Pb/^{238}U$ dates younger than 200 Ma. Ages in parentheses in A correspond to maximum depositional ages (MDAs) associated with each sample, which are displayed in Figure 2. The 310–260 Ma age domain corresponds to source terranes in the Eastern Andean metamorphic complex and the Duque de York metamorphic complex (Hervé et al., 2003). In B, the age domains "Jr" and "K1–K3" correspond with Jurassic and Cretaceous age domains defined and discussed by Pankhurst et al. (2000) and Hervé et al. (2007).

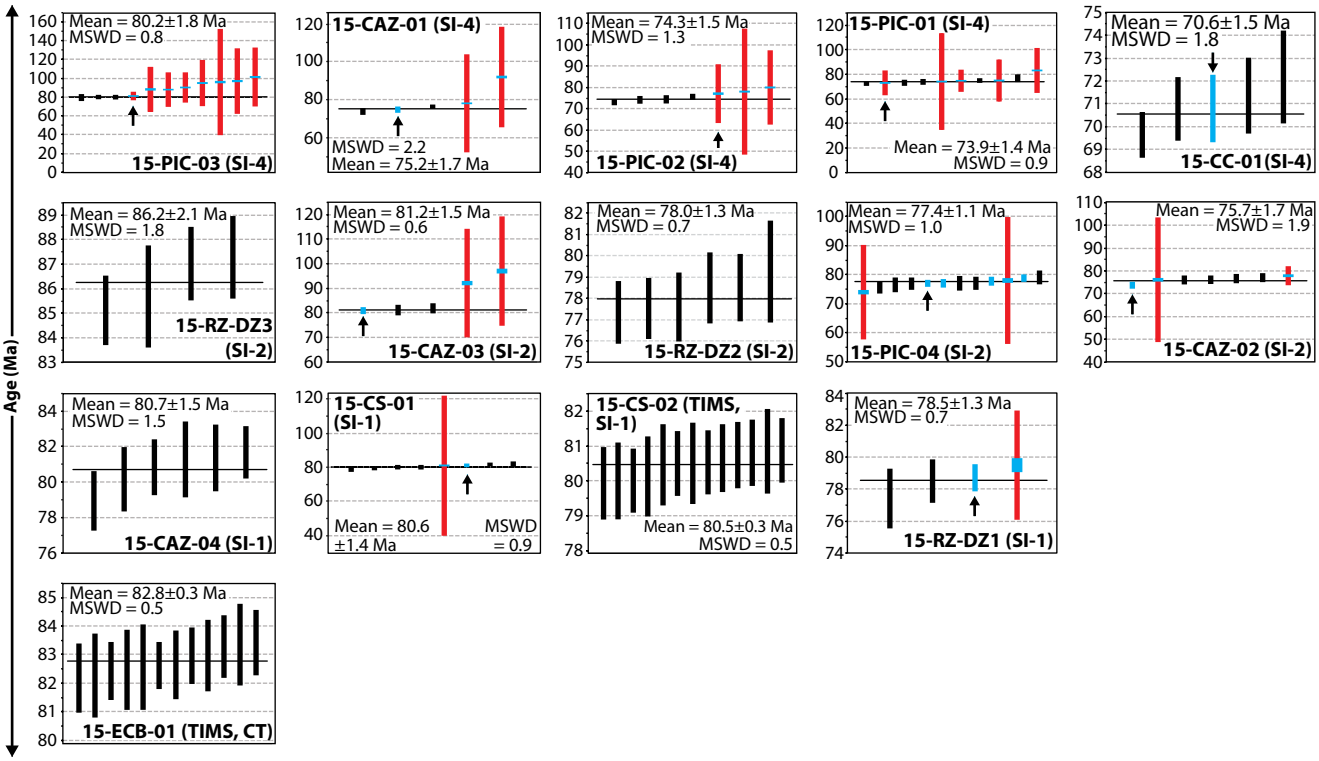

Figure 4. Weighted mean age plots that display maximum depositional ages (MDAs) obtained from the weighted mean of the youngest cluster of dates that overlap at 2σ uncertainty (YC2σ MDA calculation method). The stratigraphic interval (SI) from which each sample was obtained is listed along with the sample code (e.g., 15-PIC-03), as well as the mean square of weighted deviates (MSWD) value for each plot. Age younging direction is up and to the right. Black error bars indicate dates derived from a single analysis on a single grain. Colored error bars distinguish weighted mean ages derived from multiple measurements on a single grain. Blue error bars show age uncertainty associated with 95% confidence limits computed from the population standard deviation (σ) multiplied by 1.96 (Student's t value for an infinite number of points). This is the default uncertainty calculation in Isoplot if the dates used to generate a weighted mean age have a probability of fit >15% (Ludwig, 2012). Red error bars show age uncertainty associated with 95% confidence limits determined from the product of the Student's t result for N – 1 degrees of freedom (N—number of dates used in age calculation), σ, and the square root of the MSWD for each cluster of dates. This is the default uncertainty calculation in Isoplot if dates used to generate a weighted mean age have a probability of fit <15% (Ludwig, 2012). Colored error bars are shown together for ages where the red error bar calculation method generated a result with a very large range (e.g., 15-CS-01). Arrows indicate the weighted mean ages that were derived from the dates shown in Figure 5; these ages are MDAs derived from the youngest grain with multiple analyses (YGMA) calculation method. The second youngest grain age derived from multiple analyses was used for the YGMA calculation when the youngest grain that was analyzed multiple times yielded a very large range of possible ages via the red error bar calculation method (e.g., 15-CS-01); this could have been caused by isotopic zonation within the grain or Pb loss. Other abbreviations used in the figure: CT—Cerro Toro Formation; SI—stratigraphic interval; TIMS—thermal ionization mass spectrometry (volcanic ash samples only; Fig. 2B).

strata with several thick (>100 m) sandstone-prone turbiditic units present in numerous stratigraphic positions (Fig. 2B; Hubbard et al., 2010; Macauley and Hubbard, 2013; Pemberton et al., 2016). The sandstone-prone packages are most commonly bounded by surfaces with concave-upward, channel-form geometries in outcrop that are laterally juxtaposed against siltstone-prone strata (Macauley and Hubbard, 2013; Hubbard et al., 2014).

The upper shallow-marine deposits are correlated from Cerro Cagual to Cerro Cazador (Fig. 2). The thickness of SI-2 is consistent over much of the study area (~600 m); however, the interval thins to <300 m south of Arroyo Picana (Fig. 2B). Five sandstone samples were analyzed from this interval (Table 1). Detrital zircon dates from this interval range from 3330.2 ± 75.6 Ma to 71.2 ± 5.8 Ma (Fig. 3; Appendix 2, see footnote 1). YC2σ MDAs from this interval range from 86.2 ± 2.1 Ma to 75.7 ± 1.7 Ma (Fig. 2; Table 1).

Interpretation

The upper shallow-marine deposits represent topset deposits of a clinoform system. These topset deposits pinch out basinward to the south, and they are interpreted to genetically link to slope deposits preserved within the bulk of the underlying, mudstone-dominated clinothem succession. Off-shelf sediment delivery is recorded by sandstone-prone submarine channel-fill bodies (Macauley and Hubbard, 2013; Hubbard et al., 2014; Pemberton et al., 2016). Resistant ridges in the outcrop associated with abundant channel deposits delineate slope clinoforms characterized by elevated coarse-grained sediment flux into the basin (Hubbard et al., 2010; Romans et al.,

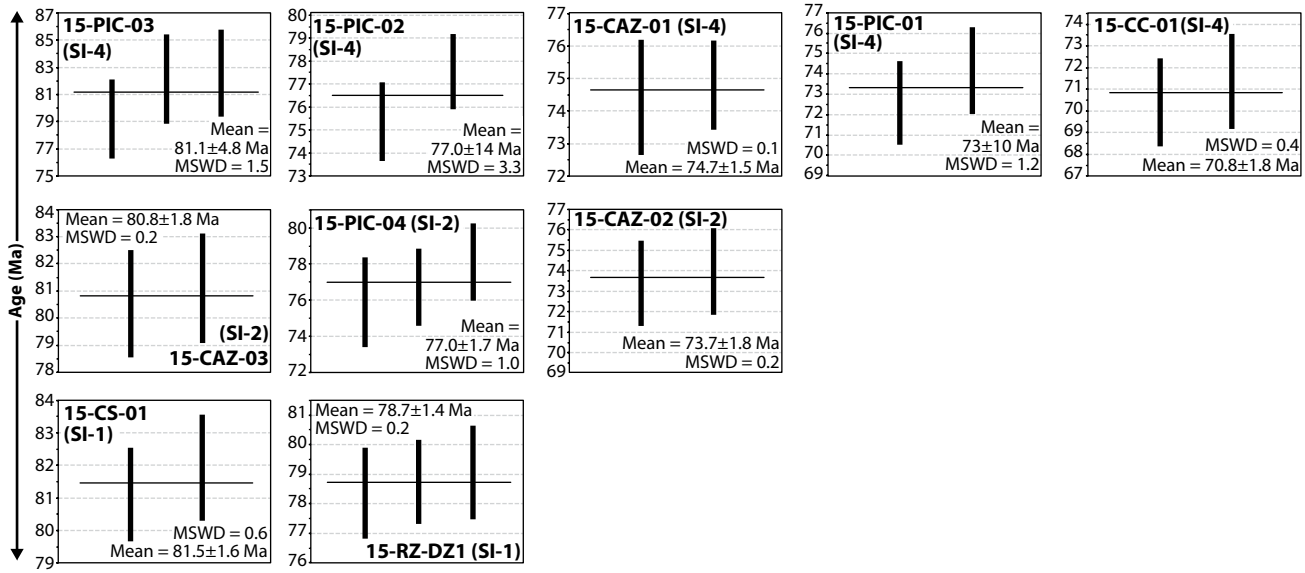

Figure 5. Weighted mean age plots that display maximum depositional ages (MDAs) calculated using a weighted mean of dates (black error bars) from the youngest grain with multiple analyses (YGMA MDA calculation method). The stratigraphic interval (SI) from which each sample was obtained is listed along with the sample code and the mean square of weighted deviates (MSWD) value for each plot. The dates in each plot were used to compute the ages that are indicated with arrows in Figure 4. The younging direction for the samples is up and to the right. Note that only samples that possessed young grains that could accommodate multiple ablation spots are displayed here.

2011). Clinoform surfaces in SI-2 have been previously documented in the southern part of the outcrop belt, and they have been estimated to exceed 900–1000 m in relief (average slope angle: 1.1°; Hubbard et al., 2010). Each successive mappable clinoform surface developed in a position markedly basinward of the previous one, which is suggestive of pronounced southward shelf-margin progradation over the life span of the depositional system associated with SI-2 (Fig. 2). The southward dip of the composite surface that defines the base of the sandstone-prone topset strata in SI-2 is consistent with a downward shelf-edge trajectory (cf. Mellere et al., 2002).

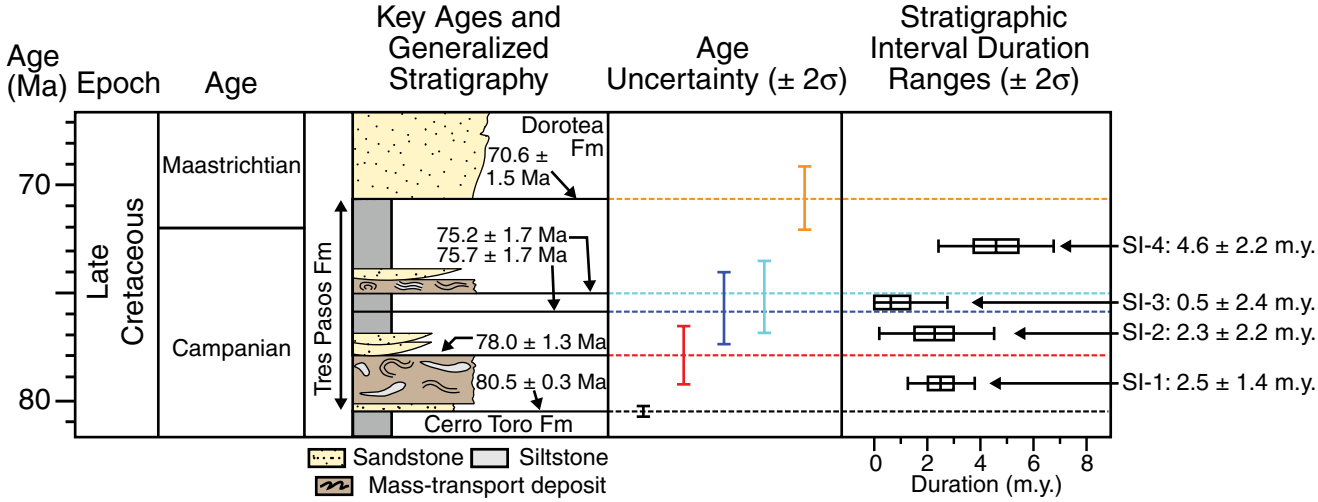

Figure 6. Schematic representation of uncertainty associated with the ages of key stratigraphic surfaces and depositional duration calculations. Key ages and stratigraphic intervals (SIs) are the same as those referenced in Figure 2. Boxes associated with each duration range denote values that are between the 1st and 3rd quartiles of the data set derived from Monte Carlo simulations; note that the data within this interquartile zone overlap with the minimum duration value for SI-3. Colored bars display the range of each data set up to 2σ. The vertical positions of the duration range error bars do not correspond to specific ages on the vertical age scale. Stratigraphic column is modified from Wilson (1991), Fildani and Hessler (2005), Fosdick et al. (2011), and Schwartz et al. (2016).

MDAs from SI-2 suggest that deposition began as early as 78.0 ± 1.3 Ma (15-RZ-DZ2) and continued until 75.7 ± 1.7 Ma (15-CAZ-02; Figs. 2B, 4, and 5). Depositional duration calculations suggest that deposition spanned 2.3 ± 2.2 m.y. (Fig. 6); the large 2σ value indicates that utilization of these MDAs and their uncertainties resulted in a wide estimate for the duration of SI-2. This result demonstrates a resolution limit for the approach followed in this study. MDAs calculated from samples 15-RZ-DZ3 and 15-CAZ-03 are older than those from underlying SI-1 deposits, and therefore they do not provide an accurate depiction of the depositional timing of SI-2 (Table 1). It is likely that the sample sizes were not large enough to obtain a significant population of approximately depositional aged zircons in these instances (Pullen et al., 2014), or that contemporaneous zircons did not enter the sediment-routing system.

Stratigraphic Interval 3 (SI-3)

The third interval of the shelf-slope succession (SI-3) is capped by resistant sandstone units that successively offlap and pinch out to the south (Fig. 2B). Overall, the underlying clinothem package is dominantly siltstone-prone with sparse thin (<5 m) sandstone-prone turbiditic units (Fig. 2B). The turbiditic units form discontinuous, resistant ridges that can be traced northward into the overlying topset deposits (Fig. 2). SI-3 is 400 m thick at Cerro Cazador, and it thins to the south (Fig. 2B). No samples were analyzed from this interval (Table 1).

Interpretation

SI-3 records the southward progradation of a clinoform system (400 m thick) to a pinch-out point on Cerro Cazador roughly coincident with the southward termination of topset sandstone in the underlying SI-2 (Fig. 2B). The presence of 400-m-thick clinothems on top of SI-2 topset strata suggests that a significant sea-level flooding surface defines the base of SI-3.

Though no samples were collected from this interval, temporal information from the top of the underlying SI-2 interval suggests that sediment delivery initiated no earlier than 75.7 ± 1.7 Ma (Figs. 4 and 5). The MDA from just above the upper boundary of SI-3 (15-CAZ-01; Figs. 2B, 4, and 5; Table 1) suggests that deposition ended no later than 75.2 ± 1.7 Ma. This suggests that sediment accumulation took place over 0.5 ± 2.4 m.y. (Fig. 6). Consequently, these MDAs provide a broad estimate for the duration of SI-3; the short time period over which the clinoform system prograded is beyond the resolution of the methods employed.

Stratigraphic Interval 4 (SI-4)

The fourth stratigraphic interval of the shelf-slope succession is dominated by thick shallow-marine deposits from central Cerro Cazador northward (Fig. 2B). To the south, the strata are characterized by dominantly siltstone-prone strata with several thick sandstone-prone turbiditic successions, 10–50 m thick, that are present along discrete stratigraphic levels (Fig. 2B). Like SI-2, these sandstone-prone packages are composite units composed of channel-form bodies that are incised into underlying siltstone-prone units (Hubbard et al., 2010; Reimchen et al., 2016). These sandstone-prone packages form resistant ridges that can be traced northward along the length of the outcrop belt into the thick shallow-marine deposits (Bauer, 2012). Notably, the transition from sandy shallow-marine deposits to more distal muddy slope deposits follows a vertical shelf-edge trajectory in the lower part of the interval (at Cerro Cazador), becoming more horizontal to the south (at Cerro Solitario; Fig. 2B). The mudstone-dominated slope succession of SI-4 thickens southwards from 400 m at Cerro Cazador to 1500 m at Arroyo Hotel, and it is composed of clinoforms with up to 1000 m relief (average slope angle: 2.0°). Five sandstone samples from SI-4 were analyzed (Table 1). Detrital zircon dates from this interval range from 3391.6 ± 71.4 Ma to 64.1 ± 4.8 Ma (Fig. 3; Appendix 2, see footnote 1). YC2σ MDAs from this interval range from 80.2 ± 1.8 Ma to 70.6 ± 1.5 Ma (Fig. 2; Table 1).

Interpretation

The southward thickening of mudstone-prone slope strata defined at the base by an abundance of sandstone records a distinct shift in slope evolution. Bauer (2012) interpreted that the clinoforms of SI-3 prograded to the relict, southernmost shelf-edge position of SI-2, which was abandoned during transgression. The abrupt change in slope relief corresponded with a period of shelf-slope instability and enhanced delivery of coarse-grained detritus beyond the shelf edge (cf. Ross et al., 1994; Prather et al., 2017). This shift initiated SI-4, providing the template for subsequent high-relief (1000 m) clinoform aggradation and progradation. Thick, traction-structured conglomerate at the base of the succession >20 km basinward of the mapped shelf-edge position is linked to sediment bypass (Stevenson et al., 2015) and establishment of sinuous submarine channel complexes (Reimchen et al., 2016).

Based on the MDA from sample 15-CAZ-01, sediment delivery associated with this interval began no later than 75.2 ± 1.7 Ma (Figs. 4 and 5). The other sample associated with the basal surface of SI-4 (15-PIC-03) yielded an MDA that is older than the SI-2 deposits and therefore does not provide insight into the onset of SI-4 sedimentation (Table 1). The youngest deposits from this interval yielded an MDA of 70.6 ± 1.5 Ma (sample 15-CC-01; Figs. 4 and 5); as a result, deposition in this interval spanned 4.6 ± 2.2 m.y. (Fig. 6). The duration of this interval is considered a minimum estimate because the upper bounding surface of this interval is not well constrained to the south of the study area.

INTEGRATION OF RESULTS

Slope System Evolution

The four stratigraphic intervals record four distinct phases of slope evolution (Fig. 7) and cumulatively represent 9.9 ± 1.4 m.y. of slope system evolution (Appendix 3, see footnote 1).

Phase 1 (SI-1) of slope evolution (2.5 ± 1.4 m.y. in duration) was characterized by episodes of significant mass wasting. Turbidity currents deposited coarse-grained detritus in topographic lows present along the rugose upper bounding surface of mass transport deposit successions. These processes can be linked to episodic periods of oversteepening and readjustment on the paleoslope (cf. Hedberg, 1970; Ross et al., 1994; Prather et al., 2017). Because the shelf edge associated with this phase is poorly constrained to the north, the nature of the proximal part of the phase 1 slope system is not deciphered.

Phase 2 (SI-2) of slope evolution (2.3 ± 2.2 m.y. in duration) was dominated by deposition of silt punctuated by several pulses of sand transport that yielded thick (>100 m) composite sandstone units. The sandstone-prone units define underlying slope clinoform surfaces in the outcrop (Hubbard et al., 2010). This stratigraphy records sediment transfer along a dominantly graded slope with short, punctuated out-of-grade phases represented by emplacement of relatively thin (<50 m) mass transport deposits and elevated coarse-grained off-shelf sediment delivery (Fig. 2B; cf. Ross et al., 1994; Pyles et al., 2011, Prather et al., 2017). This phase records a marked basinward progradation of the shelf-margin system of >65 km.

Phase 3 (SI-3) of slope evolution (0.5 ± 2.4 m.y. in duration) is characterized primarily by deposition of dominantly fine-grained sediment on low-relief (up to 400 m) slope clinoform surfaces. The transition to the deposition of fine-grained material at the onset of this phase was related to relative sea-level rise (cf. Bauer, 2012); it is interpreted that the shoreline retreated at least 20 km as a result of transgression. The graded slope clinoform surfaces in this

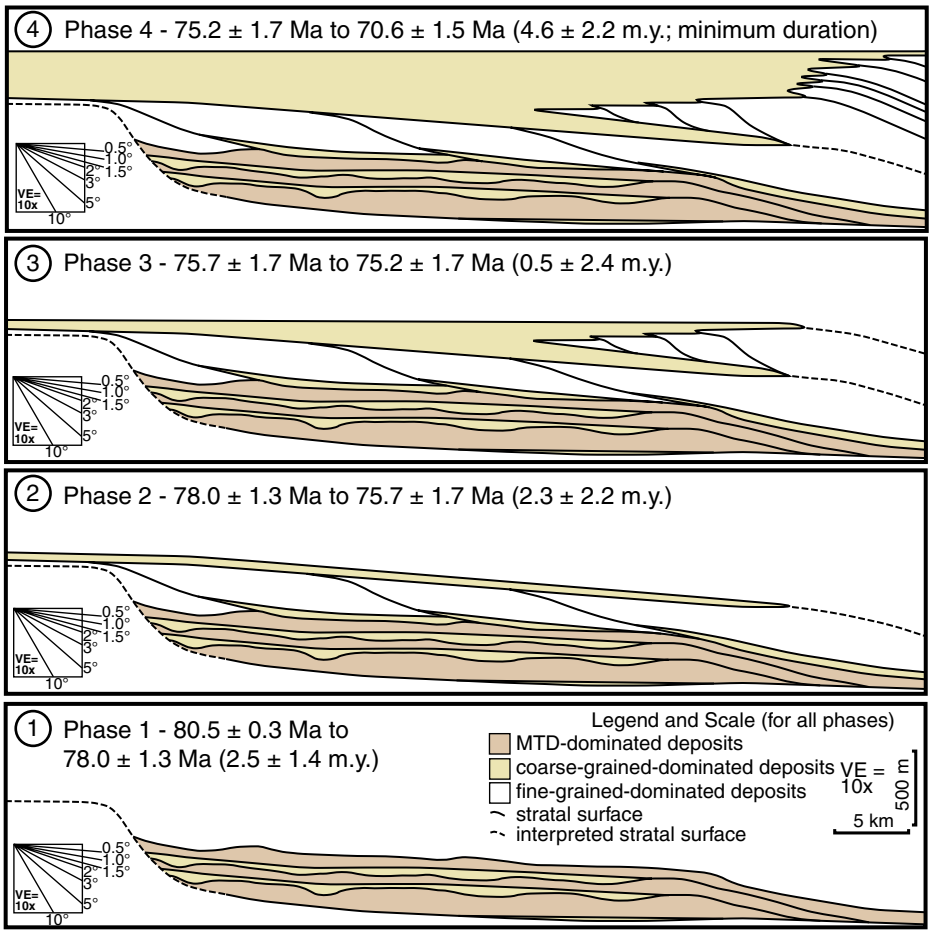

Figure 7. Evolutionary phases of the ancient slope system: (1) phase of episodic slope failure and readjustment, recorded by mass-transport deposits (MTDs) intercalated with turbiditic units that onlap onto topography generated via mass wasting; (2) pronounced progradation of high-relief (900–1000 m) clinoform surfaces with a falling shelf-edge trajectory; (3) period of sea-level rise, followed by progradation of low-relief (400 m) clinoform surfaces; and (4) a second phase of high-relief (1000 m) slope clinoform surface development, characterized by aggradation and progradation of the shelf margin. The duration associated with each phase is given in parentheses. VE—vertical exaggeration.

stratigraphic interval are dominantly progradational; the limited time over which this interval was deposited is consistent with sediment supply as a primary driver of clinoform growth (Carvajal and Steel, 2006; Carvajal et al., 2009).

Phase 4 (SI-4) of slope evolution (≥4.6 ± 2.2 m.y. in duration) is marked by a second phase of dominantly siltstone deposition with a composite, 10–60-m-thick interval composed of varying proportions of conglomerate, sandstone, and slump deposits defining the initial slope clinoform surface. As discussed, this phase was initiated as clinoforms of SI-3 prograded to the underlying, relict shelf edge of SI-2; the establishment of a particularly high-relief slope led to a period of enhanced slope instability and elevated off-shelf coarse sediment transfer. Subsequently, the majority of SI-4 records propagation of a siltstone-dominated, graded slope system. Shelf-margin growth was dominantly aggradational initially, recorded by a vertical shelf-edge trajectory, and progradational later, supported by observations of a flat shelf-edge trajectory. The SI-4 shelf margin prograded at least 35 km; progradation likely continued for at least another 15 km to the south, as lithostratigraphically equivalent topset deposits of the Dorotea Formation crop out at Sierra Dorotea (Hubbard et al., 2010; Romans et al., 2010).

Rates of Shelf-Margin Growth

Best-estimate progradation and aggradation rates for the shelf-margin system, which were determined using the mean values from each depositional duration calculation, range from 8 to 40 km/m.y. and 252 to 800 m/m.y., respectively (Fig. 8). These values fall within the range of shelf-margin growth rate values from other modern and ancient systems worldwide (Carvajal et al., 2009); the rates are most analogous to those from shelf-margin clinoforms of the Orinoco East Venezuela and Orinoco Plataforma Deltana shelf margins (Di Croce et al., 1999). Best-estimate shelf-margin growth rates experienced pronounced fluctuations over the duration of SI-2 to SI-4. From SI-2 to SI-3, the best-estimate progradation rate increases by 12 km/m.y., and the best-estimate aggradation rate increased by 539 m/m.y. (Fig. 8); these changes were likely associated with enhanced sediment delivery to the slope as a result of increased sediment supply at the SI-3 margin (Carvajal et al., 2009). From SI-3 to SI-4, the best-estimate progradation rate decreased by 32 km/m.y., while the best-estimate aggradation rate decreased by 474 m/m.y. (Fig. 8); these changes can be plausibly associated with an increase in slope relief at the SI-3–SI-4 transition, which facilitated enhanced sediment bypass downslope, as well as an increase in the scale of subsequently developed slope clinoforms (Fig. 2B). This would have led to a decline in both rates, if sediment supply to the system did not change markedly over SI-3–SI-4 time.

Though the zircon geochronology results provide a robust estimate for growth rates associated with the entire slope system analyzed (9.9 ± 1.4 m.y.), the 2σ values associated with the individual phase durations suggest that their rates could have varied considerably (Fig. 8). In particular, rates that correspond to SI-2 and SI-3 have large ranges because 2σ values associated with each duration calculation approach (e.g., SI-2 duration: 2.3 ± 2.2 m.y.) or exceed (e.g., SI-3 duration: 0.5 ± 2.4 m.y.) the magnitude of the durations of those phases. By contrast, SI-4 rates, which take place over 4.6 ± 2.2 m.y., have ranges within the bounds of previously published examples (Carvajal et al., 2009). This result demonstrates that calculation of well-constrained depositional rates for ancient sedimentary systems is only possible in instances where MDAs are precise enough to adequately resolve the depositional duration of a particular stratigraphic interval.

DISCUSSION

Controls on Slope Evolution

The length of time spanned by Tres Pasos Formation slope evolution (9.9 ± 1.4 m.y.) is comparable to second- or third-order depositional

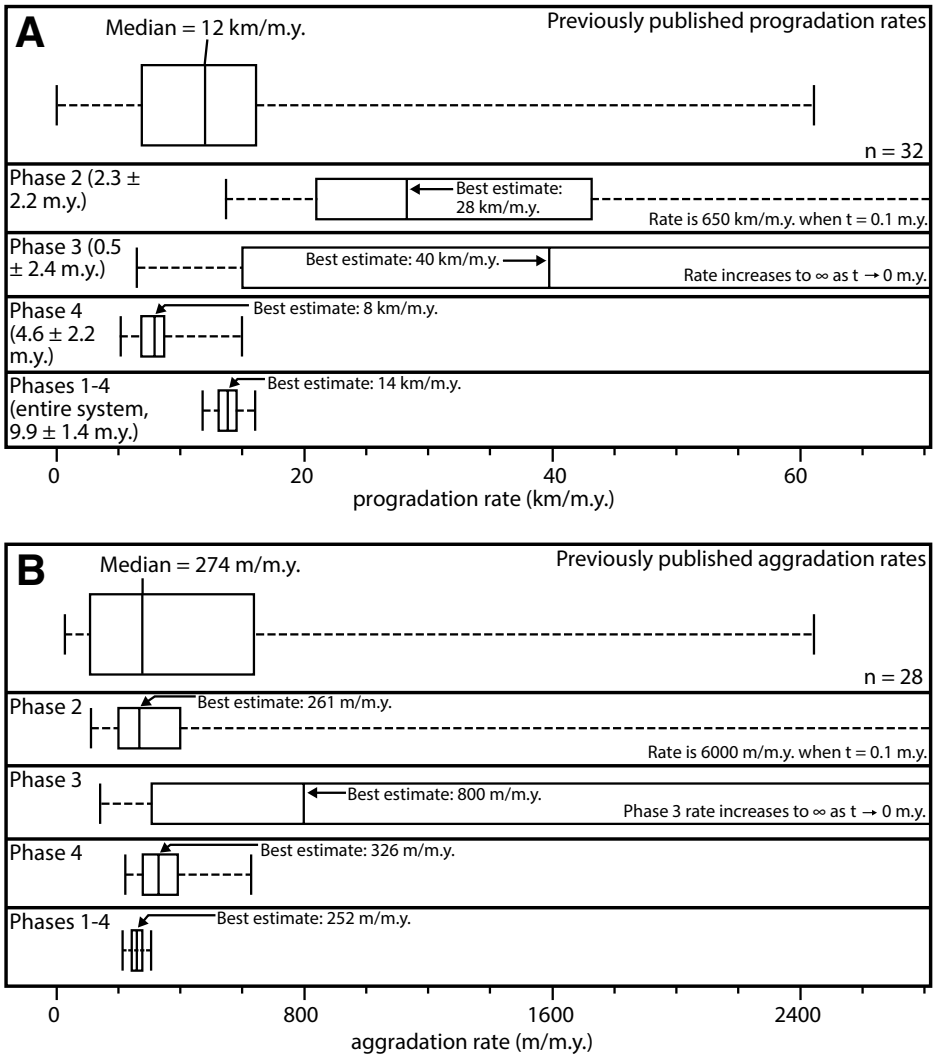

Figure 8. (A–B) Rates of shelf-margin growth. The rates of (A) progradation and (B) aggradation from each phase of slope evolution are displayed with previously published data compiled from modern and ancient continental margins worldwide (Carvajal et al., 2009, and references therein). Phase durations are provided at the left side of each plot. Boxes on each plot indicate the range of data that fall between the 1st and 3rd quartiles for each data set; box boundaries for each phase are defined by the 1st and 3rd quartile ages derived from Monte Carlo simulations (Appendix 3, see text footnote 1). Black bars indicate the range of each data set; the bars for each phase were defined by rates calculated using the maximum and minimum ages from each phase-bounding maximum depositional age (MDA). For phase rate calculations, D and T values used in each rate calculation (see Eq. 2 and Eq. 3) are as follows: phase 2: D—65 km, T—600 m; phase 3: D—20 km, T—400 m; phase 4: D—35 km, T—1500 m; phases 1–4 (entire shelf-margin system): D—140 km; T—2500 m. The updip limit of the shelf-margin system used to determine D for the phases 1–4 progradation rate calculation was the updip pinch-out of the Alta Vista Formation (i.e., Tres Pasos Formation equivalent in Argentina) near the north shore of Lago Argentino (Macellari et al., 1989). The downdip limit used to determine D for the phases 1–4 progradation rate calculation was Arroyo Hotel (Fig. 2); though the slope system does not terminate at this location, stratigraphic information southward of this point is poorly constrained. Best-estimate rates are indicated on each plot. Rates from phase 1 were not calculated because the shelf edge associated with phase 1 was not observed in the study area.

cycles in many sedimentary successions worldwide (Vail et al., 1977; Embry, 1988; Mitchum and Van Wagoner, 1991). At these time spans, controlling mechanisms might include: (1) orogenesis in the hinterland, which can impact source-to-sink configuration and sediment supply (e.g., Embry, 1988; Carvajal et al., 2009); (2) tectonically controlled variations in foreland basin subsidence (e.g., Allen and Heller, 2012); (3) eustatic sea-level change (e.g., Vail et al., 1977; Haq et al., 1987; Flint et al., 2011); (4) long-term climate variability (e.g., Boulila et al., 2011); and (5) autogenic processes, such as shelf-edge delta lobe migration (e.g., Mellere et al., 2002; Jones et al., 2015). Due to the magnitude of 2σ uncertainty values associated with each computed depositional duration, autogenic processes on shelf margins, which commonly occur on time periods that span 0.001–0.1 m.y. (Stouthamer and Berendsen, 2001), cannot be resolved using the chronologic data from this study. As a result, we interrogate the roles of allogenic controlling mechanisms that may have impacted the initiation and termination of the Tres Pasos Formation slope system.

A record of magmatism and orogenesis in the Andes of Chilean Patagonia can be gleaned from U-Pb zircon ages from Cretaceous-aged plutonic rocks of the South Patagonian Batholith (cf. Hervé et al., 2007) and from Cretaceous- to Neogene-aged deposits of the Magallanes Basin (Fig. 3; e.g., Fosdick et al., 2015; Schwartz et al., 2016; Gutiérrez et al., 2017). Campanian–Maastrichtian ages from the South Patagonian Batholith span 81–67 Ma (n = 4; Hervé et al., 2007); this indicates that arc magmatism coupled with convergence and orogenesis created young, zircon-prone material episodically over the life span of the depositional system we investigated here. Age spectra from Cretaceous–Neogene deposits in our study area and in parts of the basin to the north show largely indistinguishable populations of ages older than 84 Ma (Fig. 3; cf. Romans et al., 2010; Malkowski et al., 2017). This may imply that Andean orogenesis resulted in the exhumation and transportation of similarly aged material to the Magallanes Basin. Campanian–Maastrichtian age spectra from the detrital record contain notable population modes at 82 Ma and 70 Ma (Fig. 9). These modes are approximately coincident with the initiation and termination of the Tres Pasos Formation slope system, and they may suggest that orogenesis in the Andes associated with subduction on the western margin of South America impacted the establishment and termination of the shelf-margin system. Prolonged periods of orogenesis can facilitate rearrangement of basin-scale sediment-routing systems that originate in the hinterland (cf.

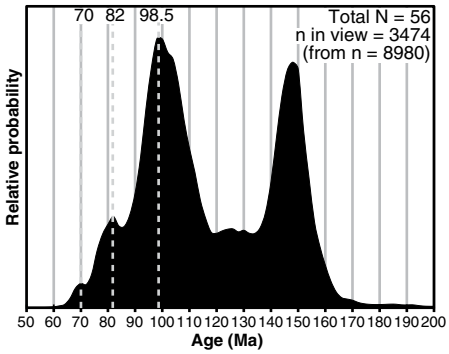

Figure 9. Probability density plot of Jurassic- and Cretaceous-aged zircons from the Magallanes Basin from localities in the vicinity of the study area (within 300 km along depositional dip) in Chilean and Argentine Patagonia. This plot integrates detrital zircon dates from this study (Fig. 3; Appendix 2, see text footnote 1), as well as from Fildani et al. (2003), Romans et al. (2010), McAtamney et al. (2011), Bernhardt et al. (2012), Fosdick et al. (2015), Malkowski et al. (2016), and Schwartz et al. (2016). Prominent age population modes from the Cenomanian–Maastrichtian are indicated with gray dashed lines.

Hoorn et al., 2010). Such a rearrangement may have encouraged storage of gravel-prone material on the shelf, rather than dispersal to deeper water. This might explain the transition from conglomerate-prone submarine channel deposits of the Cerro Toro Formation to sandstone-prone submarine channel deposits of the Tres Pasos Formation (cf. Romans et al., 2011); conglomerate is present throughout the stratigraphy, but it is preferentially preserved in updip shelf deposits in the younger depositional systems (Schwartz and Graham, 2015). Though linkage between orogenesis and slope evolution appears to be plausible, we acknowledge the potential for a lag time between magmatism and orogenesis in the hinterland, and retroarc shortening in the foreland, and subsequent rearrangement of the depositional systems (cf. DeCelles et al., 2009). Lag times associated with orogenesis and retroarc shortening in the Campanian–Maastrichtian Andes in Chilean Patagonia are poorly constrained. As such, the direct influence of orogenesis on slope evolution is difficult to decipher.

Tectonically controlled changes in Magallanes Basin subsidence rate and accommodation can be elucidated from the observed shift from deep-water deposition associated with the Punta Barrosa and Cerro Toro Formations to deposition of shelf-margin marine and continental units associated with the Tres Pasos and Dorotea Formations between ca. 81 and 70 Ma (Romans et al., 2011). Romans et al. (2011) hypothesized that this evolution records the progressive infilling of the basin, tied to a decrease in subsidence rate. The depositional system response is recorded in the transition from a dominantly canyon-fed, out-of-grade slope system (water depth: up to 2000 m; Natland et al., 1974) to one dominated by graded, progradational slope clinoform development (Hubbard et al., 2010; Romans et al., 2011). The detrital zircon age populations from the Tres Pasos and Dorotea Formations suggest that material from similar source terranes was continuously denuded in the fold-and-thrust belt through the Campanian–Maastrichtian (Figs. 3 and 9; Romans et al., 2010; Gutiérrez et al., 2017). This may have occurred via emplacement of thrust sheets composed of similar source material or by prolonged erosion of older units containing similar detrital zircon populations. Thrust fault propagation in the Campanian–Maastrichtian Andes has been evaluated via examination of faults and shear zones in the Magallanes Basin (Fosdick et al., 2011), which provided a record of thrust sheet activity, as well as the apparent migration patterns of the basin foredeep over time. These examinations, coupled with observations from the stratigraphic record, led previous workers to deduce that the position of the foredeep at the end of Cerro Toro Formation depositional time was largely similar during Tres Pasos Formation depositional time and did not begin to markedly shift eastward until ca. 74 Ma (Fosdick et al., 2011; Romans et al., 2011; Fosdick et al., 2014). This implies that thrust sheet propagation from 82 to 74 Ma was not great enough to markedly shift the foredeep position, encouraging prolonged erosion of the fold-and-thrust belt, a reduction of the tectonic load, and an overall decline in basin subsidence (cf. Beaumont, 1981; Heller et al., 1988). We interpret that this decline in subsidence was a primary slope evolution controlling mechanism, and it would have facilitated the stratigraphic evolution from the Cerro Toro Formation to the Dorotea Formation as sediment deposition outpaced basin subsidence (Hubbard et al., 2010; Romans et al., 2011).

Records of Late Cretaceous sea-level change from areas near the paleolatitude of the Magallanes Basin are not well constrained; we used the Phanerozoic global sea-level curve of Kominz et al. (2008) to investigate a potential sea-level control on slope evolution. The Campanian–Maastrichtian region of the curve shows periods of prominent sea-level rise over 82.5–81.5, 78.5–77.5, 76.0–75.5, and 70.5–69.0 Ma, and prominent sea-level fall at 81.5–78.5, 77.5–76.0, and 75.5–70.5 Ma (Fig. 10; Kominz et al., 2008). Many of the inflection points that define the boundaries between periods of sea-level rise and fall apparently coincide with the MDAs that define slope evolution phase boundaries, as well as those that define the initiation and termination of the slope system (Fig. 10). Though linkage between sea-level change and Tres Pasos Formation slope evolution seems plausible, uncertainties associated with phase-bounding MDAs (typically ±1–2 m.y.; Fig. 2B), as well as with the ages used to construct the global sea-level curve (±0.5 m.y.; Kominz et al., 2008), discourage definitive correlation between periods of eustatic sea-level rise or fall and slope evolution. Paleoclimate reconstructions based on the global $\delta^{18}O$ compilation (Friedrich et al., 2012) suggest a cooling trend from the Turonian through to the mid-Campanian (i.e., >2‰ increase over 15 m.y.) followed by comparably minor and highly variable fluctuations from mid-Campanian through the Maastrichtian (Fig. 10). However, the extent to which these global trends influenced rates of terrigenous sediment delivery (e.g., increased weathering during warmer periods) to the Magallanes Basin is unknown because of a lack of local and regional paleoclimate proxy studies.

Utility of U-Pb Zircon Geochronology for Depositional Age, Duration, and Rate Estimates

The MDA and depositional duration results provide key insights into the feasibility of zircon geochronology for the determination of depositional age, duration, and rate calculations for sedimentary systems. In this study, all sandstone-derived MDAs have 2σ uncertainty values that are >1 m.y. In all instances where a depositional duration calculation was performed using two MDAs with this level of uncertainty, the results yielded a 2σ of >2 m.y. Because most of the evolutionary phases in the Tres Pasos Formation slope system span <2.5 ± 1.4 m.y., the uncertainty values discourage precise quantification of depositional rates and their ranges. For instances where depositional durations are ≥4.6 ± 2.2 m.y. (e.g., SI-4, as well as the entire succession), rate results are within the bounds of previously published values (Carvajal et al., 2009). Upon initial inspection, this may suggest that ages computed with our detrital zircon geochronology methods are only able to reliably quantify depositional durations and rates over periods that span 4–5 m.y. at best. However, it is important to recognize that accurate and precise depositional age determination via detrital zircon geochronology principally depends upon the amount of syndepositionally formed arc-derived zircon that is incorporated into a sediment-routing system,

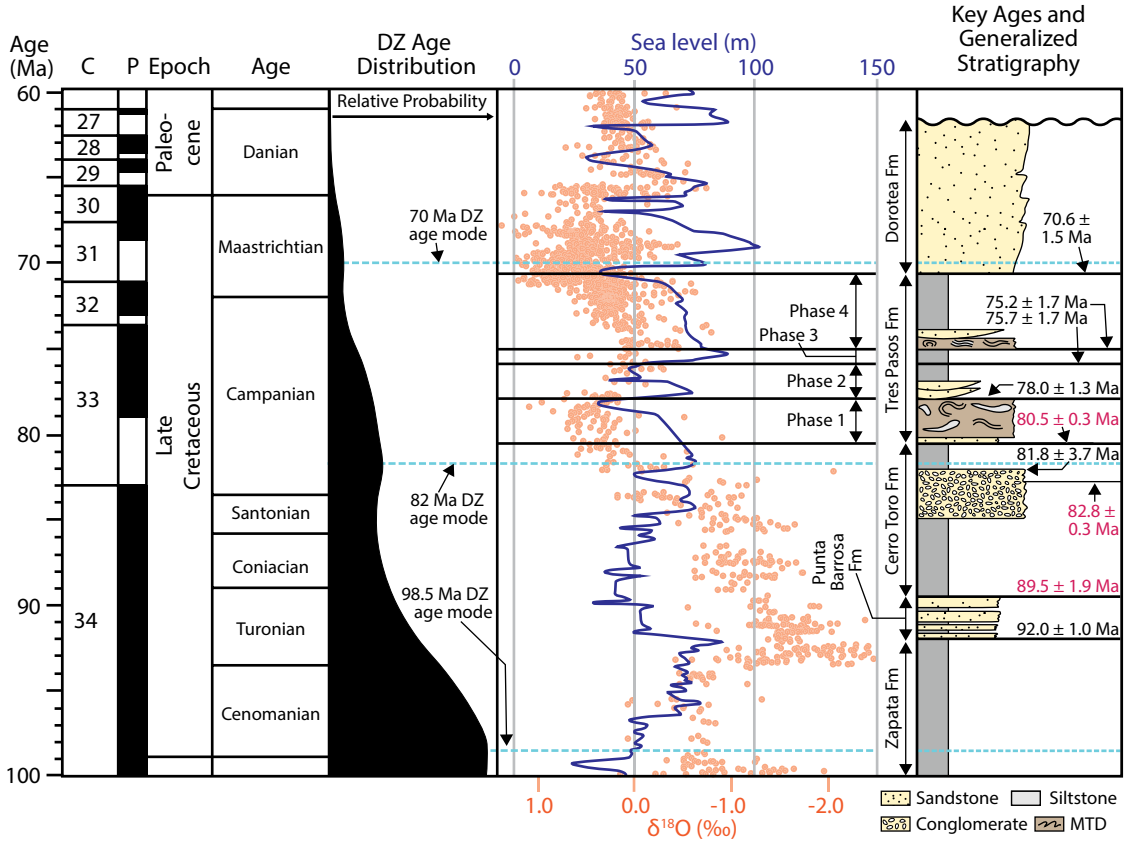

Figure 10. Compilation of zircon age data, a record of eustatic sea-level change, and oxygen isotope data from 100 to 60 Ma. C—chron; P—polarity; black and white boxes represent periods of normal and reversed polarity, respectively. The detrital zircon (DZ) age probability density plot is derived from the data presented in Figure 9. Global sea level is indicated by the blue curve (0 m—present-day sea level; Kominz et al., 2008); $\delta^{18}O$ is indicated by the orange points (Friedrich et al., 2012). Key depositional ages from Figure 2 and population modes from Figure 9 are displayed at the far right; detrital zircon maximum depositional ages (MDAs) are labeled in black, and volcanic ash zircon ages are labeled in magenta. The Punta Barrosa age (92.0 ± 1.0 Ma) is from Fildani et al. (2003), and the Cerro Toro ages (89.5 ± 1.9 Ma; 81.8 ± 3.7 Ma) are from Bernhardt et al. (2012). MTD—mass-transport deposit.

as well as the nature of sediment-routing systems that disperse the young zircon-rich material to different regions of a basin (cf. Dickinson and Gehrels, 2008; Kortyna et al., 2014). Many sedimentary basins that are adjacent to active volcanic arcs (e.g., forearc, backarc, and foreland basins) receive large volumes of young arc-derived zircon-rich material from the hinterland over their life spans (Cawood et al., 2012). If large amounts of young arc-derived zircon are distributed to all parts of a basin over its life span, a computed MDA from any depositional setting in that basin may employ a large number of zircon dates that are approximately coincident with the TDA. If the dates used to calculate the age significantly overlap at 2σ uncertainty (i.e., probability of fit that approaches 100%), the precision of the computed age may improve and facilitate enhanced age resolution for depositional duration and rate estimates (cf. Schoene et al., 2013). If only a small proportion of this young, syndepositionally formed material is distributed to a certain part of a basin, the MDA derived from the deposits in that region may only employ a small number of dates that may not significantly overlap at 2σ uncertainty (i.e., probability of fit that approaches 0%). This would negatively impact the accuracy and precision of the measurement and discourage meaningful quantification of depositional duration and rates. Therefore, comprehensive knowledge of the amount of young, syndepositionally formed zircon produced, coupled with a thorough understanding of the distribution of this material across the basin, is required to properly assess whether any zircon geochronology technique will generate an accurate and precise depositional age that can be used in duration and rate estimates. This suggests that though our techniques are unable to resolve time periods shorter than 4 m.y. in the Magallanes Basin, they may be more appropriate for use for duration and rate estimates in basins that receive greater amounts of syndepositionally formed zircon.

Furthermore, the evaluation of MDA uncertainty reveals that the geologic period or era over which a sedimentary system was active may also impact calculation of duration and rate estimates using MDAs from detrital zircons. Depositional age precision, which is mathematically defined as the percentage related to the quotient of the 2σ uncertainty and the weighted mean age for a given MDA, ranges between 1.4% and 2.4% for each sandstone sample in this study (Table 1). Consider a scenario where MDAs of similar precision were computed for a sedimentary system that was active during the Early Ordovician (485.4–470.0 Ma; duration: 15.4 m.y.). In this

case, the MDAs that define the lower and upper bounds of the interval would have absolute 2σ uncertainties that would span ±6.6–11.6 m.y., and computed duration and rate estimates may have large ranges. As a result, one must evaluate whether their analytical method of choice can work within the resolution of not only the length of time spanned by deposition, but also for the geologic time over which the system was active.

CONCLUSIONS

Evaluation of stratigraphic and zircon-derived U-Pb age data reveals new insight into the evolution of a Campanian–Maastrichtian shelf-slope system in the Magallanes Basin in southern Chile. Integration of new stratigraphic information and >6600 new U-Pb zircon (detrital and volcanic ash) ages reveals a four-phase evolutionary framework associated with a largely progradational shelf-margin system. The evolutionary framework is dominated by graded slope clinoforms, punctuated by periods of out-of-grade slope development in which coarse-grained sediment delivery to basinward zones was enhanced. Individual slope evolutionary phases spanned 0.5 ± 2.4 m.y. to 4.6 ± 2.2 m.y. in duration, while evolution of the entire system spanned 9.9 ± 1.4 m.y. (80.5 ± 0.3 Ma to 70.6 ± 1.5 Ma). We infer that slope evolution was largely driven by an overall decline in basin subsidence related to lack of thrust sheet propagation in the adjacent fold-and-thrust belt from 82 to 74 Ma.

The results of this study have significant implications regarding the use of detrital zircon geochronology to compute depositional ages, durations, and rates in ancient sedimentary systems. We showed that our methods can provide reliable estimates of depositional duration for time periods that span >4 m.y. in the Magallanes Basin; estimates for shorter time periods are fraught with too much uncertainty to yield meaningful results. The usefulness of a given depositional duration and rate estimate for a particular stratigraphic interval is principally related to the accuracy and precision of each MDA used in the calculation; MDA accuracy and precision are strongly linked to the number of syndepositionally formed zircons employed in the MDA calculation, and the similarity in age between those zircons. Where feasible, comparison of detrital zircon ages with other independent measurements of depositional age from a nearby stratigraphic unit (e.g., volcanic ash ages, biostratigraphic markers), coupled with high-resolution stratigraphic mapping over great distances (e.g., >100 km), can greatly enhance interpretations of whether detrital zircons will be able to suitably approximate the depositional age of a unit.

We deduce that depositional age, duration, and rate estimation based on detrital zircon geochronology that employs LA-ICP-MS is probably most effective in the proximal regions of arc-related sedimentary basins (e.g., forearc, backarc) that receive abundant amounts of syndepositionally formed zircon-rich detritus from the hinterland continuously over their life spans. Furthermore, we infer that detrital zircon geochronology techniques can only effectively determine depositional durations and rates in ancient systems in instances where the magnitude of uncertainty on each bounding MDA does not approach the magnitude of the length of time being evaluated. In general, the absolute uncertainty associated with U-Pb ages from sources that are Paleozoic and older is larger compared to the uncertainty related to ages that are Mesozoic and younger (i.e., 2.0% uncertainty on 300 Ma age = ±6 m.y.). Therefore, robust depositional duration and rate constraints for systems active during these time periods may only be possible over 10–100 m.y. scales using methods analogous to those documented here.

ACKNOWLEDGMENTS

The funding for this work was generously provided by the industrial sponsors of the Chile Slope Systems Joint Industry Project (BHP Billiton, Chevron, ConocoPhillips, Hess, Nexen, Repsol, Shell, and Statoil), a Natural Sciences and Engineering Research Council of Canada (NSERC) Discovery Grant (RGPIN/341715-2013) to Hubbard, and by the University of Calgary Silver Anniversary Fellowship and Queen Elizabeth II graduate scholarships to Daniels. We are grateful to various landowners for granting access to the outcrops, including Hotel Explora, the Alarcón family, Mauricio Álvarez Kusanovic and Hella Roehrs Jeppesen, Armando Álvarez Saldivia, Jose Antonio Kusanovic, and Tamara Mac Leod, as well as Christian Cárdenas Alvarado and Raúl Cárdenas Rodríguez. We are grateful to Tomislav Goic and Alejandrina Mac Leod for friendship and support during our field work. We thank Daniel Hill, Sebastian Kaempfe, and Zane Jobe for their assistance collecting samples, as well as Dominic Armitage, Sarah Jancuska, Daniel Niquet, Erin Pemberton, Aaron Reimchen, and Sarah Southern for providing paleocurrent data. We also thank Dave Barbeau, Mihai Ducea, and Zirchron Geoscience Services for help with the thermal ionization mass spectrometry analyses. Finally, we are thankful for reviews and comments from Carita Augustsson, David Chew, Associate Editor Peter Cawood, and Science Editor Aaron Cavosie, which greatly enhanced the clarity and quality of the manuscript.

REFERENCES CITED

Allen, P.A., and Heller, P.L., 2012, Dispersal and preservation of tectonically generated alluvial gravels in sedimentary basins, *in* Busby, C., and Perez, A.A., eds., Tectonics of Sedimentary Basins: Recent Advances: Chichester, UK, Wiley-Blackwell Publishing, p. 111–130, doi:10.1002/9781444347166.ch6.

Arbe, H.A., and Hechem, J.J., 1984, Estratigrafía y facies de depósitos marinos profundos del Cretácico Superior, Lago Argentino, Provincia de Santa Cruz: IX Congreso Geológico Argentino Actas, v. 5, p. 7–41.

Armitage, D.A., Romans, B.W., Covault, J.A., and Graham, S.A., 2009, The influence of mass-transport deposit surface topography on the evolution of turbidite architecture: The Sierra Contreras, Tres Pasos Formation (Cretaceous), southern Chile: Journal of Sedimentary Research, v. 79, p. 287–301, doi:10.2110/jsr.2009.035.

Auchter, N.C., Romans, B.W., and Hubbard, S.M., 2016, Influence of deposit architecture on intrastratal deformation, slope deposits of the Tres Pasos Formation, Chile: Sedimentary Geology, v. 341, p. 13–26, doi:10.1016/j.sedgeo.2016.05.005.

Bain, H.A., and Hubbard, S.M., 2016, Stratigraphic evolution of a long-lived submarine channel system in the Late Cretaceous Nanaimo Group, British Columbia, Canada: Sedimentary Geology, v. 337, p. 113–132, doi:10.1016/j.sedgeo.2016.03.010.

Bauer, D.B., 2012, Stratigraphic Evolution of a High-Relief Slope Clinoform System, Magallanes Basin, Chilean Patagonia [M.Sc. thesis]: Calgary, Canada, University of Calgary, 130 p.

Beaumont, C., 1981, Foreland basins: Geophysical Journal of the Royal Astronomical Society, v. 65, p. 291–329, doi:10.1111/j.1365-246X.1981.tb02715.x.

Bernhardt, A., Jobe, Z.R., Grove, M., and Lowe, D.R., 2012, Palaeogeography and diachronous infill of an ancient deep-marine foreland basin, Upper Cretaceous Cerro Toro Formation, Magallanes Basin: Basin Research, v. 24, p. 269–294, doi:10.1111/j.1365-2117.2011.00528.x.

Boulila, S., Galbrun, B., Miller, K.G., Pekar, S.F., Browning, J.V., Laskar, J., and Wright, J.D., 2011, On the origin of Cenozoic and Mesozoic "third-order" eustatic sequences: Earth-Science Reviews, v. 109, p. 94–112, doi:10.1016/j.earscirev.2011.09.003.

Bruhn, R.L., and Dalziel, I.W.D., 1977, Destruction of the Early Cretaceous marginal basin in the Andes of Tierra del Fuego, *in* Talwani, M., and Pitman, W.C., eds., Island Arcs, Deep Sea Trenches and Back-Arc Basins: Washington, D.C., American Geophysical Union, Maurice Ewing Series 1, p. 395–405, doi:10.1029/ME001p0395.

Calderón, M., Fosdick, J.C., Warren, C., et al., 2012, The low-grade Canal de las Montañas shear zone and its role on the tectonic emplacement of the Sarmiento ophiolitic complex and Late Cretaceous Patagonian Andes orogeny, Chile: Tectonophysics, v. 524–525, p. 165–185, doi:10.1016/j.tecto.2011.12.034.

Callec, Y., Deville, E., Desaubliaux, G., Griboulard, R., Huyghe, P., Mascle, A., Mascle, G., Noble, M., Padron de Carillo, C., and Schmitz, J., 2010, The Orinoco turbidite system: Tectonic controls on sea-floor morphology and sedimentation: American Association of Petroleum Geologists Bulletin, v. 94, p. 869–887, doi:10.1306/11020909021.

Carvajal, C.R., and Steel, R.J., 2006, Thick turbidite successions from supply-dominated shelves during sea-level highstand: Geology, v. 34, p. 665–668, doi:10.1130/G22505.1.

Carvajal, C.R., and Steel, R.J., 2009, Shelf-edge architecture and bypass of sand to deep water: Influence of shelf-edge processes, sea level, and sediment supply: Journal of Sedimentary Research, v. 79, p. 652–672, doi:10.2110/jsr.2009.074.

Carvajal, C.R., Steel, R.K., and Petter, A.L., 2009, Sediment supply: The main driver of shelf-margin growth: Earth-Science Reviews, v. 79, p. 652–672.

Cawood, P.A., Hawkesworth, C.J., and Dhuime, B., 2012, Detrital zircon record and tectonic setting: Geology, v. 40, p. 875–878, doi:10.1130/G32945.1.

Clift, P.D., and Gaedicke, C., 2002, Accelerated mass flux to the Arabian Sea during the middle-late Miocene: Geology, v. 30, p. 207–210, doi:10.1130/0091-7613(2002)030<0207:AMFTTA>2.0.CO;2.

Coleman, J.M., and Prior, D.B., 1988, Mass-wasting on continental margins: Annual Review of Earth and Planetary Sciences, v. 16, p. 101–119, doi:10.1146/annurev.ea.16.050188.000533.

Covault, J.A., Romans, B.W., and Graham, S.A., 2009, Outcrop expression of a continental-margin-scale

shelf-edge delta from the Cretaceous Magallanes Basin, Chile: Journal of Sedimentary Research, v. 79, p. 523–539, doi:10.2110/jsr.2009.053.

Covault, J.A., Romans, B.W., Fildani, A., McGann, M., and Graham, S.A., 2010, Rapid climatic signal propagation from source to sink in a southern California sediment-routing system: The Journal of Geology, v. 118, p. 247–259, doi:10.1086/651539.

Dalziel, I.W.D., 1986, Collision and Cordilleran orogenesis: An Andean perspective, *in* Coward, M.P., and Ries, A.C., eds., Collision Tectonics: Geological Society, London, Special Publication 19, p. 389–404.

Dalziel, I.W.D., de Wit, M.J., and Palmer, K.F., 1974, Fossil marginal basin in the southern Andes: Nature, v. 250, p. 291–294, doi:10.1038/250291a0.

Daniels, B.G., 2015, Downslope Characterization of Channel Fill and Stratigraphic Architecture along an Ancient Basin Margin, Tres Pasos Formation, Southern Chile [M.S. thesis]: Calgary, Canada, University of Calgary, 160 p.

Davis, D.W., Williams, L.S., and Krogh, T.E., 2003, Historical development of zircon geochronology, *in* Hancha, J.M., and Hoskin, P.W.O., eds., Zircon: Chantilly, Virginia, Mineralogical Society of America, Reviews in Mineralogy and Geochemistry, v. 53, p. 145–181.

DeCelles, P.G., Ducea, M.N., Kapp, P., and Zandt, G., 2009, Cyclicity in Cordilleran orogenic systems: Nature Geoscience, v. 2, p. 251–257, doi:10.1038/ngeo469.

de Wit, M.J., and Stern, C.R., 1981, Variations in the degree of crustal extension during formation of a back-arc basin: Tectonophysics, v. 72, p. 229–260, doi:10.1016/0040-1951(81)90240-7.

Dickinson, W.R., and Gehrels, G.E., 2008, U-Pb ages of detrital zircons in relation to paleogeography: Triassic paleodrainage networks and sediment dispersal across southwest Laurentia: Journal of Sedimentary Research, v. 78, p. 745–764, doi:10.2110/jsr.2008.088.

Dickinson, W.R., and Gehrels, G.E., 2009, Use of U-Pb ages of detrital zircons to infer maximum depositional ages of strata: A test against a Colorado Plateau Mesozoic database: Earth and Planetary Science Letters, v. 288, p. 115–125, doi:10.1016/j.epsl.2009.09.013.

Di Croce, J., Bally, A.W., and Vail, P., 1999, Sequence stratigraphy of the eastern Venezuelan Basin, *in* Mann, P., ed., Sedimentary Basins of the World, Volume 4: Amsterdam, Elsevier, p. 419–476.

Dixon, J.F., Steel, R.J., and Olariu, C., 2012, River-dominated, shelf-edge deltas: Delivery of sand across the shelf break in the absence of slope incision: Sedimentology, v. 59, p. 1133–1157, doi:10.1111/j.1365-3091.2011.01298.x.

Dott, R.H., Winn, R.D., Jr., and Smith, C.H.L., 1982, Relationship of late Mesozoic and early Cenozoic sedimentation to the tectonic evolution of the southernmost Andes and the Scotia arc, *in* Craddock, C., ed., Antarctic Geoscience: Madison, Wisconsin, University of Wisconsin Press, p. 193–202.

Embry, A.F., 1988, Triassic sea-level changes: Evidence from the Canadian Arctic archipelago, *in* Wilgus, C.K., Hastings, B.S., Posamentier, H.W., Van Wagoner, J.C., Ross, C.A., and Kendall, C.G.St.C., eds., Sea-Level Changes: An Integrated Approach: Society of Economic Paleontologists and Mineralogists (SEPM) Special Publication 42, p. 249–259.

Fedo, C.M., Sircombe, K.N., and Rainbird, R.H., 2003, Detrital zircon analysis of the sedimentary record, *in* Hanchar, H.M., and Hoskin, P.W.O., eds., Zircon: Chantilly, Virginia, Mineralogical Society of America, Reviews in Mineralogy and Geochemistry, v. 53, p. 277–303, doi:10.2113/0530277.

Fildani, A., and Hessler, A.M., 2005, Stratigraphic record across a retroarc basin inversion: Rocas Verdes–Magallanes Basin, Patagonian Andes: Geological Society of America Bulletin, v. 117, p. 1596–1614, doi:10.1130/B25708.1.

Fildani, A., Cope, T.D., Graham, S.A., and Wooden, J.L., 2003, Initiation of the Magallanes foreland basin: Timing of the southernmost Patagonian Andes orogeny revised by detrital zircon provenance analysis: Geology, v. 31, p. 1081–1084, doi:10.1130/G20016.1.

Fildani, A., Drinkwater, N.J., Weislogel, A., McHargue, T., Hodgson, D.M., and Flint, S.M., 2007, Age controls on the Tanqua and Laingsburg deep-water systems: New insights on the evolution and sedimentary fill of the Karoo Basin, South Africa: Journal of Sedimentary Research, v. 77, p. 901–908, doi:10.2110/jsr.2007.088.

Fletcher, S.D.T., 2013, Stratigraphic Characterization of a Cretaceous Slope Channel Complex in the Tres Pasos Formation, Arroyo Picana–Laguna Figueroa Outcrop Belt, Chilean Patagonia [M.S. thesis]: Calgary, Canada, University of Calgary, 119 p.

Flint, S.S., Hodgson, D.M., Sprague, A.R., Brunt, R.L., Van der Merwe, W.C., Figueiredo, J., Prélat, A., Box, D., Di Celma, C., and Kavanagh, J.P., 2011, Depositional architecture and sequence stratigraphy of the Karoo Basin floor to shelf edge succession, Laingsburg depocentre, South Africa: Marine and Petroleum Geology, v. 28, p. 658–674, doi:10.1016/j.marpetgeo.2010.06.008.

Fosdick, J.C., Romans, B.W., Fildani, A., Bernhardt, A., Calderón, M., and Graham, S.A., 2011, Kinematic evolution of the Patagonian retro-arc fold-and-thrust belt and Magallanes foreland basin, Chile and Argentina, 51°30′S: Geological Society of America Bulletin, v. 123, p. 1679–1698, doi:10.1130/B30242.1.

Fosdick, J.C., Graham, S.A., and Hilley, G.E., 2014, Influence of attenuated lithosphere and sediment loading on flexure of the deep-water Magallanes retroarc foreland basin, Southern Andes: Tectonics, v. 33, p. 2505–2525, doi:10.1002/2014TC003684.

Fosdick, J.C., Grove, M., Graham, S.A., Hourigan, J.K., Lovera, O., and Romans, B.W., 2015, Detrital thermochronologic record of burial heating and sediment recycling in the Magallanes foreland basin, Patagonian Andes: Basin Research, v. 27, p. 546–572, doi:10.1111/bre.12088.

Friedrich, O., Norris, R.D., and Erbacher, J., 2012, Evolution of middle to Late Cretaceous oceans—A 55 m.y. record of Earth's temperature and carbon cycle: Geology, v. 40, p. 107–110, doi:10.1130/G32701.1.

Gehrels, G.E., 2012, Detrital zircon U-Pb geochronology: Current methods and new opportunities, *in* Busby, C., and Perez, A.A., eds., Tectonics of Sedimentary Basins: Chichester, UK, Wiley-Blackwell Publishing, p. 45–62, doi:10.1002/9781444347166.ch2.

Gehrels, G.E., Valencia, V.A., and Ruiz, J., 2008, Enhanced precision, accuracy, efficiency, and spatial resolution of U-Pb ages by laser ablation–multicollector–inductively coupled plasma–mass spectrometry: Geochemistry Geophysics Geosystems, v. 9, Q03017, doi:10.1029/2007GC001805.

Gutiérrez, N.M., Le Roux, J.P., Vásquez, A., Carreño, C., Pedroza, V., Araos, J., Oyarzún, J.L., Pablo Pino, J., Rivera, H.A., and Hinojosa, L.F., 2017, Tectonic events reflected by palaeocurrents, zircon geochronology, and palaeobotany in the Sierra Baguales of Chilean Patagonia: Tectonophysics, v. 695, p. 76–99, doi:10.1016/j.tecto.2016.12.014.

Hadler-Jacobsen, F., Johannessen, E.P., Ashton, N., Henriksen, S., Johnson, S.D., and Kristensen, J.B., 2005, Submarine fan morphology and lithology distribution: A predictable function of sediment delivery, gross shelf-to-basin relief, slope gradient, and basin topography, *in* Doré, A.G., and Vining, B.A., eds., Petroleum Geology: North-West Europe and Global Perspectives—Proceedings of the 6th Conference: London, Geological Society, p. 1121–1145, doi:10.1144/0061121.

Haq, B.U., Hardenbol, J., and Vail, P.R., 1987, Chronology of fluctuating sea levels since the Triassic: Science, v. 235, p. 1156–1167, doi:10.1126/science.235.4793.1156.

Hedberg, H.D., 1970, Continental margins from viewpoint of the petroleum geologist: American Association of Petroleum Geologists Bulletin, v. 54, p. 3–43.

Heller, P.L., Angevine, C.L., Winslow, N.S., and Paola, C., 1988, Two-phase stratigraphic model of foreland-basin sequences: Geology, v. 16, p. 501–504, doi:10.1130/0091-7613(1988)016<0501:TPSMOF>2.3.CO;2.

Hervé, F., Pankhurst, R.J., and Fanning, C.M., 2003, Detrital zircon age patterns and provenance of the metamorphic complexes of southern Chile: Journal of South American Earth Sciences, v. 16, p. 107–123, doi:10.1016/S0895-9811(03)00022-1.

Hervé, F., Pankhurst, R.J., Fanning, C.M., Calderón, M., and Yaxley, G.M., 2007, The South Patagonian batholith: 150 my of granite magmatism on a plate margin: Lithos, v. 97, p. 373–394, doi:10.1016/j.lithos.2007.01.007.

Hoorn, C., Wesselingh, F.P., ter Steege, H., et al., 2010, Amazonia through time: Andean uplift, climate change, landscape evolution, and biodiversity: Science, v. 330, p. 927–931, doi:10.1126/science.1194585.

Horstwood, M.S.A., Košler, J., Gehrels, G., et al., 2016, Community-derived standards for LA-ICP-MS U-(Th-)Pb geochronology—Uncertainty propagation, age interpretation and data reporting: Geostandards and Geoanalytical Research, v. 40, p. 311–332, doi:10.1111/j.1751-908X.2016.00379.x.

Houseknecht, D.W., Bird, K.J., and Schenk, C.J., 2009, Seismic analysis of clinoform depositional sequences and shelf-margin trajectories in Lower Cretaceous (Albian) strata, Alaska North Slope: Basin Research, v. 21, p. 644–654, doi:10.1111/j.1365-2117.2008.00392.x.

Hubbard, S.M., Romans, B.W., and Graham, S.A., 2008, Deep-water foreland basin deposits of the Cerro Toro Formation, Magallanes Basin, Chile: Architectural elements of a sinuous basin axial channel belt: Sedimentology, v. 55, p. 1333–1359, doi:10.1111/j.1365-3091.2007.00948.x.

Hubbard, S.M., Fildani, A., Romans, B.W., Covault, J.A., and McHargue, T.R., 2010, High-relief slope clinoform development: Insights from outcrop, Magallanes Basin, Chile: Journal of Sedimentary Research, v. 80, p. 357–375, doi:10.2110/jsr.2010.042.

Hubbard, S.M., Covault, J.A., Fildani, A., and Romans, B.W., 2014, Sediment transfer and deposition in slope channels: Deciphering the record of enigmatic deep-sea processes from outcrop: Geological Society of America Bulletin, v. 126, p. 857–871, doi:10.1130/B30996.1.

Johannessen, E.P., and Steel, R.J., 2005, Shelf-margin clinoforms and prediction of deepwater sands: Basin Research, v. 17, p. 521–550, doi:10.1111/j.1365-2117.2005.00278.x.

Jones, G.E.D., Hodgson, D.M., and Flint, S.S., 2015, Lateral variability in clinoform trajectory, process regime, and sediment dispersal patterns beyond the shelf-edge rollover in exhumed basin margin-scale clinothems: Basin Research, v. 27, p. 657-680, doi:10.1111/bre.12092.

Kominz, M.A., Browning, J.V., Miller, K.G., Sugarman, P.J., Mizintseva, S., and Scotese, C.R., 2008, Late Cretaceous to Miocene sea-level estimates from the New Jersey and Delaware coastal plain coreholes: An error analysis: Basin Research, v. 20, p. 211–226, doi:10.1111/j.1365-2117.2008.00354.x.

Kortyna, C., Donaghy, E., Trop, J.M., and Idleman, B., 2014, Integrated provenance record of a forearc basin modified by slab-window magmatism: Detrital-zircon geochronology and sandstone compositions of the Paleogene Arkose Ridge Formation, south-central Alaska: Basin Research, v. 26, p. 436–460, doi:10.1111/bre.12033.

Ludwig, K.R., 1998, On the treatment of concordant uranium-lead ages: Geochimica et Cosmochimica Acta, v. 62, p. 665–676, doi:10.1016/S0016-7037(98)00059-3.

Ludwig, K.R., 2012, Manual for Isoplot 3.75: Berkeley Geochronology Center Special Publication 5, revised 30 January 2012, 75 p.

Macauley, R.V., and Hubbard, S.M., 2013, Slope channel sedimentary processes and stratigraphic stacking, Cretaceous Tres Pasos Formation slope system, Chilean Patagonia: Marine and Petroleum Geology, v. 41, p. 146–162, doi:10.1016/j.marpetgeo.2012.02.004.

Macellari, C.E., 1988, Late Cretaceous Kossmaticeratidae (Ammonoidea) from the Magallanes Basin, Chile: Journal of Paleontology, v. 62, p. 889–905, doi:10.1017/S002233600003016X.

Macellari, C.E., Barrio, C.A., and Manassero, M.J., 1989, Upper Cretaceous to Paleocene depositional sequences and sandstone petrography of southwestern Patagonia (Argentina and Chile): Journal of South American Earth Sciences, v. 2, p. 223–239, doi:10.1016/0895-9811(89)90031-X.

Malkowski, M.A., Grove, M., and Graham, S.A., 2016, Unzipping the Patagonian Andes—Long-lived influence of rifting history on foreland basin evolution: Lithosphere, v. 8, p. 23–28, doi:10.1130/L489.1.

Malkowski, M.A., Schwartz, T.M., Sharman, G.R., Sickmann, Z.T., and Graham, S.A., 2017, Stratigraphic and provenance variations in the early evolution of the Magallanes-Austral foreland basin: Implications for the role of

longitudinal versus transverse sediment dispersal during arc-continent collision: Geological Society of America Bulletin, v. 129, p. 349–371, doi:10.1130/B31549.1.

Martinsen, O.J., Bøen, F., Charnock, M.A., Mangerud, G., and Nøttvedt, A., 1999, Cenozoic development of the Norwegian margin 60–64°N: Sequences and sedimentary response to variable basin physiography and tectonic setting, *in* Fleet, A.J., and Boldy, S.A.R., Petroleum Geology: North-West Europe and Global Perspectives—Proceedings of the 5th Conference: London, Geological Society, p. 293–304, doi:10.1144/0050293.

Masson, D.G., Harbitz, C.B., Wynn, R.B., Pedersen, G., and Løvholt, F., 2006, Submarine landslides: Processes, triggers and hazard prediction: Royal Society of London Philosophical Transactions, ser. A, v. 364, p. 2009–2039, doi:10.1098/rsta.2006.1810.

Matthews, W.A., and Guest, B., 2017, A practical approach for collecting large-*n* detrital zircon U-Pb data sets by quadrupole LA-ICP-MS: Geostandards and Geoanalytical Research, v. 41, no. 2, p. 161–180, doi:10.1111/ggr.12146.

Mayall, M., Jones, E., and Casey, M., 2006, Turbidite channel reservoirs—Key elements in facies prediction and effective development: Marine and Petroleum Geology, v. 23, p. 821–841, doi:10.1016/j.marpetgeo.2006.08.001.

McAtamney, J., Klepeis, K., Mehrtens, C., Thomson, S., Betka, P., Rojas, L., and Snyder, S., 2011, Along-strike variability of back-arc basin collapse and the initiation of sedimentation in the Magallanes foreland basin, southernmost Andes (53–54.5°S): Tectonics, v. 30, TC5001, doi:10.1029/2010TC002826.

McHugh, C.M.G., Damuth, J.E., Gartner, S., Katz, M.E., and Mountain, G.S., 1996, Oligocene to Holocene mass-transport deposits of the New Jersey continental margin and their correlation to sequence boundaries, *in* Mountain, G.S., Miller, K.G., Blum, P., Poag, C.W., and Twichell, D.C., eds., Proceedings of the Ocean Drilling Program, Scientific Results, Volume 150: College Station, Texas, Ocean Drilling Program, p. 189–228.

Mellere, D., Plink-Björklund, P., and Steel, R.J., 2002, Anatomy of shelf deltas at the edge of a prograding Eocene shelf margin, Spitsbergen: Sedimentology, v. 49, p. 1181–1206.

Mitchum, R.M., Jr., and Van Wagoner, J.C., 1991, High-frequency sequences and their stacking patterns: Sequence-stratigraphic evidence of high-frequency eustatic cycles: Sedimentary Geology, v. 70, p. 131–160, doi:10.1016/0037-0738(91)90139-5.

Mukasa, S.B., and Dalziel, I.W.D., 1996, Southernmost Andes and South Georgia Island, North Scotia Ridge, zircon U-Pb and muscovite $^{40}Ar/^{39}Ar$ age constraints on tectonic evolution of southwestern Gondwanaland: Journal of South American Earth Sciences, v. 9, p. 349–365, doi:10.1016/S0895-9811(96)00019-3.

Mulder, T., Ducassou, E., Gillet, H., et al., 2014, First discovery of channel-levee complexes in a modern deep-water carbonate slope environment: Journal of Sedimentary Research, v. 84, p. 1139–1146, doi:10.2110/jsr.2014.90.

Mutti, E., and Normark, W.R., 1987, Comparing examples of modern and ancient turbidite systems: Problems and concepts, *in* Legget, J.K., and Zuffa, G.G., eds., Deep Water Clastic Deposits: Models and Case Histories: London, Graham and Trotman, p. 1–38, doi:10.1007/978-94-009-3241-8_1.

Natland, M.L., González, E., Cañón, A., and Ernst, M., 1974, A System of Stages for Correlation of Magallanes Basin Sediments: Geological Society of America Memoir 139, 126 p., doi:10.1130/MEM139-p1.

Nelson, C.H., Damuth, J.E., and Twichell, D.C., 2011, Interplay of mass-transport and turbidite-system deposits in different active tectonic and passive continental margin settings: External and local controlling factors, *in* Shipp, C.R., Weimer, P., and Posamentier, H.W., eds., Mass-Transport Deposits in Deepwater Settings: Society for Sedimentary Geology (SEPM) Special Publication 96, p. 39–66.

Otamendi, J.E., Ducea, M.N., Tibaldi, A.M., Bergantz, G.W., de la Rosa, J.D., and Vujovich, G.I., 2009, Generation of tonalitic and dioritic magmas by coupled partial melting of gabbroic and metasedimentary rocks within the deep crust of the Famatinian magmatic arc, Argentina: Journal of Petrology, v. 50, p. 841–873, doi:10.1093/petrology/egp022.

Pankhurst, R.J., Riley, T.R., Fanning, C.M., and Kelley, S.P., 2000, Episodic silicic volcanism in Patagonia and Antarctic Peninsula: Chronology of magmatism associated with the break-up of Gondwana: Journal of Petrology, v. 41, p. 605–625, doi:10.1093/petrology/41.5.605.

Pemberton, E.A.L., Hubbard, S.M., Fildani, A., Romans, B.W., and Stright, L., 2016, The stratigraphic expression of decreasing confinement along a deep-water sediment routing system: Outcrop example from southern Chile: Geosphere, v. 12, p. 114–134, doi:10.1130/GES01233.1.

Petter, A.L., Steel, R.J., Mohrig, D., Kim, W., and Carvajal, C.R., 2013, Estimation of the paleoflux of terrestrial-derived solids across ancient basin margins using the stratigraphic record: Geological Society of America Bulletin, v. 125, p. 578–593, doi:10.1130/B30603.1.

Pinous, O.V., Levchuk, M.A., and Sahagian, D.L., 2001, Regional synthesis of the productive Neocomian complex of West Siberia: Sequence stratigraphic framework: American Association of Petroleum Geologists Bulletin, v. 85, p. 1713–1730.

Piper, D.J.W., 1975, Late Quaternary deep-water sedimentation off Nova Scotia and western Grand Banks: Calgary, Alberta, *in* Yorath, C.J., Parker, E.R., and Glass, D.J., eds., Canada's Continental Margins and Offshore Petroleum Exploration: Canadian Society of Petroleum Geologists Memoir 4, p. 195–204.

Piper, D.J.W., and Normark, W.R., 1989, Late Cenozoic sea-level changes and the onset of glaciation: Impact on continental slope progradation off eastern Canada: Marine and Petroleum Geology, v. 6, p. 336–347, doi:10.1016/0264-8172(89)90030-5.

Plink-Björklund, P., Steel, R., and Mellere, D., 2001, Turbidite variability and architecture of sand-prone, deep-water slopes: Eocene clinoforms in the Central Basin, Spitsbergen: Journal of Sedimentary Research, v. 71, p. 895–912, doi:10.1306/030501710895.

Porębski, S., and Steel, R.J., 2003, Shelf-margin deltas: Their stratigraphic significance and relation to deepwater sands: Earth-Science Reviews, v. 62, p. 283–326, doi:10.1016/S0012-8252(02)00161-7.

Prather, B.E., O'Byrne, C., and Pirmez, C., 2017, Sediment partitioning, continental slopes and base-of-slope systems: Basin Research, v. 29, no. 3, p. 394–416, doi:10.1111/bre.12190.

Pullen, A., Ibáñez-Mejía, M., Gehrels, G.E., Ibáñez-Mejía, J.C., and Pecha, M., 2014, What happens when n = 1000? Creating large-*n* geochronological datasets with LA-ICP-MS for geologic investigations: Journal of Analytical Atomic Spectrometry, v. 29, p. 971–980, doi:10.1039/C4JA00024B.

Pyles, D.R., Syvitsky, J.P.M., and Slatt, R.M., 2011, Defining the concept of stratigraphic grade and applying it to stratal (reservoir) architecture and evolution of the slope-to-basin profile: An outcrop perspective: Marine and Petroleum Geology, v. 28, p. 675–697, doi:10.1016/j.marpetgeo.2010.07.006.

Rabinowitz, P.D., and La Brecque, J., 1979, The Mesozoic South Atlantic Ocean and evolution of its continental margin: Journal of Geophysical Research, v. 84, p. 5973–6002, doi:10.1029/JB084iB11p05973.

Ramos, V.A., 1988, The tectonics of the Central Andes: 30°–33°S latitude, *in* Clark, S.P., Burchfiel, B.C., and Suppe, J., eds., Processes in Continental Lithospheric Deformation: Geological Society of America Special Paper 218, p. 31–54, doi:10.1130/SPE218-p31.

Reimchen, A.P., Hubbard, S.M., Stright, L., and Romans, B.W., 2016, Using sea-floor morphometrics to constrain stratigraphic models of sinuous submarine channel systems: Marine and Petroleum Geology, v. 77, p. 92–115, doi:10.1016/j.marpetgeo.2016.06.003.

Rich, J.L., 1951, Three critical environments of deposition and criteria for recognition of rocks deposited in each of them: Geological Society of America Bulletin, v. 62, p. 1–20, doi:10.1130/0016-7606(1951)62[1:TCEODA]2.0.CO;2.

Romans, B.W., and Graham, S.A., 2013, A deep-time perspective of land-ocean linkages in the sedimentary record: Annual Review of Marine Science, v. 5, p. 69–94, doi:10.1146/annurev-marine-121211-172426.

Romans, B.W., Hubbard, S.M., and Graham, S.A., 2009, Stratigraphic evolution of an outcropping continental slope system, Tres Pasos Formation at Cerro Divisadero, Chile: Sedimentology, v. 56, p. 737–764, doi:10.1111/j.1365-3091.2008.00995.x.

Romans, B.W., Fildani, A., Graham, S.A., Hubbard, S.M., and Covault, J.A., 2010, Importance of predecessor basin history on the sedimentary fill of a retroarc foreland basin: Provenance analysis of the Cretaceous Magallanes Basin, Chile (50–52°S): Basin Research, v. 22, p. 640–658, doi:10.1111/j.1365-2117.2009.00443.x.

Romans, B.W., Fildani, A., Hubbard, S.M., Covault, J.A., Fosdick, J.C., and Graham, S.A., 2011, Evolution of deep-water stratigraphic architecture, Magallanes Basin, Chile: Marine and Petroleum Geology, v. 28, p. 612–628, doi:10.1016/j.marpetgeo.2010.05.002.

Romans, B.W., Castelltort, S., Covault, J.A., Fildani, A., and Walsh, J.P., 2016, Environmental signal propagation in sedimentary systems across timescales: Earth-Science Reviews, v. 153, p. 7–29, doi:10.1016/j.earscirev.2015.07.012.

Ross, W.C., Halliwell, B.A., May, J.A., Watts, D.E., and Syvitski, J.P.M., 1994, Slope readjustment: A new model for the development of submarine fans and aprons: Geology, v. 22, p. 511–514, doi:10.1130/0091-7613(1994)022<0511:SRANMF>2.3.CO;2.

Rubio-Cisneros, I.I., and Lawton, T.F., 2011, Detrital zircon U-Pb ages of sandstones in continental red beds at Valle de Huizachal, Tamaulipas, NE Mexico: Record of Early–Middle Jurassic arc volcanism and transition to crustal extension: Geosphere, v. 7, p. 159–170, doi:10.1130/GES00567.1.

Saleeby, J.B., Sams, D.B., and Kistler, R.W., 1987, U/Pb zircon, strontium, and oxygen isotopic and geochronological study of the southernmost Sierra Nevada Batholith, California: Journal of Geophysical Research, v. 92, p. 10,443–10,466, doi:10.1029/JB092iB10p10443.

Schoene, B., Condon, D.J., Morgan, L., and McLean, N., 2013, Precision and accuracy in geochronology: Elements, v. 9, p. 19–24, doi:10.2113/gselements.9.1.19.

Schwartz, T.M., and Graham, S.A., 2015, Stratigraphic architecture of a tide-influenced delta, Upper Cretaceous Dorotea Formation, Magallanes-Austral Basin, Patagonia: Sedimentology, v. 62, p. 1039–1077, doi:10.1111/sed.12176.

Schwartz, T.M., Fosdick, J.C., and Graham, S.A., 2016, Using detrital zircon U-Pb ages to calculate Late Cretaceous sedimentation rates in the Magallanes-Austral basin, Patagonia: Basin Research (in press), doi:10.1111/bre.12198.

Shultz, M.R., Fildani, A., Cope, T.D., and Graham, S.A., 2005, Deposition and stratigraphic architecture of an outcropping ancient slope system: Tres Pasos Formation, Magallanes Basin, southern Chile, *in* Hodgson, D.M., and Flint, S.S., eds., Submarine Slope Systems: Processes and Products: Geological Society, London, Special Publication 244, p. 27–50.

Sláma, J., and Košler, J., 2012, Effects of sampling and mineral separation on accuracy of detrital zircon studies: Geochemistry Geophysics Geosystems, v. 13, Q05007, doi:10.1029/2012GC004106.

Smith, C.H.L., 1977, Sedimentology of the Late Cretaceous (Santonian-Maastrichtian) Tres Pasos Formation, Ultima Esperanza District, Southern Chile [M.S. thesis]: Madison, Wisconsin, University of Wisconsin, 129 p.

Spencer, C.J., Kirkland, C.L., and Taylor, R.J.M., 2016, Strategies towards statistically robust interpretations of in situ U-Pb zircon geochronology: Geoscience Frontiers, v. 7, p. 581–589, doi:10.1016/j.gsf.2015.11.006.

Stern, C.R., and de Wit, M.J., 2003, Rocas Verdes ophiolites, southernmost South America: Remnants of progressive stages of development of oceanic-type crust in a continental margin back-arc basin, *in* Dilek, Y., and Robinson, P.T., eds., Ophiolites in Earth History: Geological Society, London, Special Publication 218, p. 665–683, doi:10.1144/GSL.SP.2003.218.01.32.

Stern, C.R., Mukasa, S.B., and Fuenzalida, R., 1992, Age and petrogenesis of the Sarmiento ophiolite complex of southern Chile: Journal of South American Earth Sciences, v. 6, p. 97–104, doi:10.1016/0895-9811(92)90020-Y.

Stevenson, C.J., Jackson, C.A.L., Hodgson, D.M., Hubbard, S.M., and Eggenhuisen, J.T., 2015, Deep-water sediment bypass: Journal of Sedimentary Research, v. 85, p. 1058–1081, doi:10.2110/jsr.2015.63.

Stouthamer, E., and Berendsen, H.J.A., 2001, Avulsion frequency, avulsion duration, and interavulsion period of Holocene channel belts in the Rhine-Meuse delta, the Netherlands: Journal of Sedimentary Research, v. 71, p. 589–598, doi:10.1306/112100710589.

Uchupi, E., and Emery, K.O., 1967, Structure of continental margin off Atlantic Coast of United States: American Association of Petroleum Geologists Bulletin, v. 51, p. 223–234.

Vail, P.R., Todd, R.G., and Sangree, J.B., 1977, Seismic stratigraphy and global changes in sea level: Part 5. Chronostratigraphic significance of seismic reflections: Section 2. Application of seismic reflection configuration to stratigraphic interpretation, *in* Payton, C.E., ed., Seismic Stratigraphy—Applications to Hydrocarbon Exploration: American Association of Petroleum Geologists Memoir 26, p. 99–116.

Weimer, P., and Pettingill, H.S., 2007, Global overview of deep-water exploration and production, *in* Nilsen, T.H., Shew, R.D., Steffens, G.S., and Studlick, J., eds., Atlas of Deep-Water Outcrops: American Association of Petroleum Geologists Studies in Geology 56, p. 7–11.

Wilson, T.J., 1991, Transition from back-arc to foreland basin development in the southernmost Andes: Stratigraphic record from the Ultima Esperanza District, Chile: Geological Society of America Bulletin, v. 103, p. 98–111, doi:10.1130/0016-7606(1991)103<0098:TFBATF>2.3.CO;2.

Winn, R.D., and Dott, R.H.J., 1979, Deep-water fan-channel conglomerates of Late Cretaceous age, southern Chile: Sedimentology, v. 26, p. 203–228, doi:10.1111/j.1365-3091.1979.tb00351.x.

Wynn, R.B., Masson, D.G., Stow, D.A.V., and Weaver, P.P.E., 2000, The Northwest African slope apron: A modern analogue for deep-water systems with complex seafloor topography: Marine and Petroleum Geology, v. 17, p. 253–265, doi:10.1016/S0264-8172(99)00014-8.

Science Editor: Aaron J. Cavosie
Associate Editor: Peter A. Cawood

Manuscript Received 24 January 2017
Revised Manuscript Received 4 May 2017
Manuscript Accepted 14 July 2017

Printed in the USA